

博士論文（要約）

Numerical and experimental study on failure mode classification of piping components under seismic loading

(地震荷重を受ける配管構造物の破損モード分類に関する
解析および実験による研究)

バリ モハマド アブドラ アル

Abstract

Preparation for Beyond Design Basis Events (BDBE) becomes an important issue as the lessons learned from the Fukushima Daiichi nuclear accident. IAEA propose Design Extension Condition (DEC) to consider BDBE. New defense in depth concept includes DEC in the plant status which means, DEC cases need to be considered in the design of a plant. DEC can occur due to extreme loading. One of the extreme loading is excessive seismic load. From a view point of structural design, the strength evaluation approach for DEC is somewhat different from conventional one for design basis accident (DBA). For DEC cases, the best estimate approach is essential to realize rational countermeasure. For best estimation of structural strength against seismic load, it is required to know the dominant failure modes of the structure to make adequate preparation against seismic loading.

Ratcheting, collapse and fatigue are the probable failure modes under seismic loading. Because of several different failure modes candidate due to seismic loading, it is helpful to put the occurrence conditions of all these failure modes in a same plot which can be named as failure mode map. The current studies describe an attempt to make a failure mode map due to seismic loading which includes the ratcheting, collapse and fatigue failure modes. A combined experimental and numerical approach is adopted to investigate the failure modes in beam shape model. A dynamic nonlinear elastic-plastic finite element analysis has been carried out to evaluate the occurrence condition of failure modes under bending-bending (primary-secondary loading) loading condition at various frequencies of acceleration. The beam model was tested on a shaking table with similar loading condition as numerical analysis. The results of the experimental analyses validate the numerical model. For ratcheting the analysis results were compared with Yamashita et al. theoretical bending-bending ratcheting model and as well a

results those obtained from experimental analysis. A good analogy has been found between the FEA results and theoretical results. Experimental and finite element analyses were also carried out for collapse. So far, the first phase of fatigue experiment has done.

After that, the similar finite element method is used to investigate the failure modes of an elbow pipe model. Ratcheting and collapse was analyzed and a good coherence of results has been found between a beam model and an elbow pipe model. Furthermore, this study tries to characterize the seismic loading phenomena as the characteristics of seismic loading are bit unclear. It has found that at low frequency seismic loading is act like load-controlled loading and at relatively high frequency it acts more like displacement-controlled loading.

Finally all the occurrence conditions of ratcheting, collapse and fatigue were put in the failure mode map by using non dimensional stress parameters as used in the Bree diagram. The concept of a failure mode map gives a useful classification tool against seismic loading for the designers of nuclear components.

Table of Contents

Abstract	ii
Table of Contents	iv
List of Figures	vi
Chapter 1 - Introduction.....	1
1-1 Design basis accident and design extension condition.....	1
1-2 Seismic PRA.....	4
1-2-1 Seismic hazard analysis.....	5
1-2-2 Components and piping fragility assessment	6
1-2-3 Accident sequence analysis and risk evaluation.....	7
1-3 Characteristics of seismic load	9
1-4 Failure modes under seismic loadings.....	10
1-4-1 EPRI piping and fitting dynamic reliability tests[40]	11
1-4-2 Large scale piping system tests[43][46][47][48].....	14
1-4-3 Trial model tests of pipes under excessive seismic loads[44]	17
1-4-4 Fundamental experimental studies under seismic loading[16]	21
1-4-5 Probable failure modes due to seismic loading	24
1-5 Objectives of the present study.....	24
1-6 Outline of the thesis.....	26
Chapter 2 - Methodology	27
2-1 Analytical approach with finite element method.....	27
2-1-1 Beam model for understanding of basic mechanisms	27
2-1-2 Material properties of beam	29
2-1-3 Loading and analysis conditions of beam	31
2-1-4 Elbow pipe model for applicability validation of applicability to piping	33
2-1-5 Material properties of elbow pipe	35
2-1-6 Loading and analysis conditions of elbow pipe	36
2-2 Experimental approach.....	38
2-2-1 Experimental specimen and material	38

List of Figures

2-2-2 Shaking table and other instruments	42
2-2-3 Experimental procedure	45
Chapter 3 - Ratcheting Failure Mode.....	47
3-1 Theory of Ratcheting.....	47
3-1-1 Bree Diagram [56].....	48
3-1-2 Bending-bending ratchet diagram [64].....	52
3-1-3 Treatment of seismic loading	57
3-2 Finite element analyses of beam models	58
3-3 Dynamic experiments of beam models	63
3-3-1 Experimental conditions of beam models	63
3-4 FE analyses of elbow pipe models	67
Chapter 4 - Other Failure Modes	71
4-1 Collapse	71
4-2 Fatigue	72
Chapter 5 - Conclusions and Future Work	72
6-1 Conclusions	72
6-1-1 Frequency dependent characteristics of seismic loading	73
6-1-2 Failure mode map for dominant failure modes	74
6-1-3 Applicability of simple beam model diagrams to complicated elbow pipe model	75
6-2 Future works	77
References	78
Acknowledgements.....	89

List of Figures

Figure 1-1 Consideration of severe accidents in design [14]	2
Figure 1-2 Typical seismic hazard curve [30].....	6
Figure 1-3 Typical fragility curve [32]	7
Figure 1-4 Difference of characteristics of load-controlled and displacement-controlled loading [9]	10
Figure 1-5 In-plane elbow test setup[40].....	12
Figure 1-6 In-plane tee test setup [40].....	13
Figure 1-7 Input seismic motion time history[40].....	13
Figure 1-8 Input strain time history showing ratcheting behavior [40]	14
Figure 1-9 Time history of seismic input wave [48]	15
Figure 1-10 Elbow specimen for dynamic tests [43]	16
Figure 1-11 Large scale piping system model [43]	16
Figure 1-12 Fatigue lives through the piping component tests [48]	17
Figure 1-13 Inverted type specimen [44]	18
Figure 1-14 Pendant-weight type specimen [44]	19
Figure 1-15 Sinusoidal waves with tapered part [44]	20
Figure 1-16 Input seismic wave [44].....	20
Figure 1-17 Progress of ratchet collapse failure mode observed in the inverted type specimen.....	21
Figure 1-18 Failure mode observed in the pendant-weight type specimen	21
Figure 1-19 Possible failure modes under extreme seismic load	22
Figure 1-20 Fundamental vibration test experimental setup.....	23
Figure 1-21 Obtained Failure modes from fundamental vibration strength tests.....	24
Figure 2-1 Meshes of the beam model.....	28
Figure 2-2 Elastic-perfectly-plastic material model [57]	31
Figure 2-3 Loading and boundary condition of the beam model	32
Figure 2-4 Geometry and dimensions of pipe.....	34
Figure 2-5 Pure lead stress strain diagram.....	36

Figure 2-6 Trial model tests experimental setup (a) Dimensions and loading (b) Photograph of real experiment [46].....	37
Figure 2-7 Experimental setup followed by FEM setup.....	38
Figure 2-8 Configuration of beam shaped specimen for experiment.....	39
Figure 2-9 Experimental setup	39
Figure 2-10 Stress-strain curves of typical structural material (a & b) and simulated materials (Pb-Sb) alloys (c) [58].....	41
Figure 2-11 Vibration testing machine	42
Figure 2-12 Vibration testing machine operation	43
Figure 2-13 Data logger (Keyence) used in this experiment	43
Figure 2-14 Acceleration pickup (red circle) attached with shaking table.....	45
Figure 3-1 Bree diagram for a thin tube [56]	50
Figure 3-2 Prototypical stress-strain behaviors for an elastic-plastic material in the classic Bree problem [65]	51
Figure 3-3 Rectangular-beam model for ratcheting [64]	52
Figure 3-4 Relationship between deflection and bending moment [64].....	55
Figure 3-5 Ratchet diagram for rectangular beam [64]	56
Figure 3-6 Ground acceleration and floor response acceleration	57
Figure 3-7 Typical input acceleration for ratcheting analyses	63
Figure 3-13 Detailed dimension of experimental setup	65
Figure 6-1 Proposed ratchet diagram with theoretical lines.....	73
Figure 6-2 Proposed failure mode map.....	75

List of Tables

Table 1-1 Level of Defence in Depth [16].....	3
Table 2-1 Geometry of the beam model.....	28
Table 2-2 The summary of Element type 'PlaseStress (Quad 4)' [54]	29
Table 2-3 Material data for elastic plastic analysis of beam.....	30
Table 2-4 Dimensions of elbow pipe and support beam.....	34
Table 2-5 Summary of element type 'Shell (Quad 4)' [54]	35
Table 2-6 Material properties of Pb (99%) - Sb (1%)	41
Table 3-1 Analyses conditions of ratcheting of beam model.....	61
Table 3-2 Experimental analyses conditions for ratcheting for beam model.....	66
Table 3-3 Analysis conditions of ratcheting of elbow model.....	68

Chapter 1 - Introduction

1-1 Design basis accident and design extension condition

On March 11, 2011, a 9.0-magnitude earthquake struck Japan and was followed by about 15 m tsunami, resulting in extensive damage to the nuclear power reactors at the Fukushima Dai-ichi facility[1]. After the accident at Fukushima Daiichi Nuclear Power Station several investigation committees issued reports with lessons learned from the accident[2][3][4][5][6][7][8]. Among those lessons, some recommendations have been made on beyond design basis accident (BDBA) research[9][10]. Design basis accidents (DBA)[11] in nuclear power plants are well studied and safety requirements are well established for many years. Regulatory bodies around the world have been set the design and safety guidelines for DBA cases. Experience has shown that the probability of occurrence of DBA during the lifetime of a nuclear plant is high though the impact on the plant is relatively low, due to this, the ‘design basis’ consider conservative approach[12]. Some events can occur outside of design basis cases which are termed as BDBA. BDBA has a low probability of occurrence but a very high impact on the plant. IAEA proposed design extension condition (DEC)[13] for considering a part of BDBA that can occur due to extreme loading, shown in Fig.1.

According to the IAEA definition, design extension conditions are:

Postulated accident conditions that are not considered for design basis accidents, but that are considered in the design process of the facility in accordance with best estimate methodology, and for which releases of radioactive material are kept within acceptable limits. Design extension

conditions could include conditions in events without significant fuel degradation and conditions with core melting.

IAEA NS-R-1 (2000) Safety of Nuclear Power Plants: Design

Operational states		Accidental conditions	
Normal Operation	Anticipated operational occurrence	Design basis accidents	Beyond design basis accidents
Plant status			Accident management



IAEA SSR-2/1 (2012) Safety of Nuclear Power Plant: Design Specific Safety Requirements

Operational states		Accidental conditions		Conditions practically eliminated
Normal Operation	Anticipated operational occurrence	Design basis accidents (Conservative calculation)	Design extension conditions (Best estimation)	
Plant status (consider in design)				

Figure 1-1 Consideration of severe accidents in design [14]

On the other hand, conventionally, Defence in Depth (DiD), has been used as a basic idea of nuclear safety, includes "prevention and control of abnormality", "Control of design basis accidents" and "Mitigation of Accident Impact" are the pillars, mainly focusing on "preventing the occurrence of abnormalities". However, after the Fukushima Daiichi Nuclear Power Plant accident, the DiD has also been revised and placed design extension conditions in level four [14]. Table 1 is showing the updated DiD with its specific objectives and essential design means of each level.

Table 1-1 Level of Defence in Depth [16]

Level of defence	Objective	Essential design means
Level 1	Prevention of abnormal operation and failures	Conservative design and high quality in construction of normal operation systems, including monitoring and control systems
Level 2	Control of abnormal operation and detection of failures	Limiting and protection systems and other surveillance features
Level 3	Control of design basis accidents (postulated single initiating events)	Engineered safety features (safety systems)
Level 4	Control of design extension conditions (postulated multiple failures events) including prevention of accident progression and mitigation of the consequences of severe accidents	Safety features for design extension conditions
Level 5	Mitigation of radiological consequences of significant releases of radioactive materials	On-site and off-site emergency response facilities

Current structure of level four of DiD deals with the control of all postulated multiple failures with and without core melt. The essential means of achieving the objective of level four include safety systems for DEC and accident management procedure and guidelines. However, the design of safety systems for DEC is different from design basis cases. Instead of taking the conservative approach as for DBA, DEC adopts best estimation technique [15]. From the structural point of view, the design of structure and components needs to be improved to prevent the accidents and

progression of accidents during the DEC cases. DEC generally occurs at extreme loading (i.e. high temperature, pressure or excessive seismic loading) [16]. And the frequencies of these events are very less. So to postulate and realize the possible structural failure at extreme loading, it is necessary for the designer to know the possible failure modes. For the best estimation approach[17], it is also required to clarify the dominant failure. Clarification of dominant failure modes includes the identification of probable failure modes as well as the occurrence conditions of these failure modes. Certain loading conditions can induce more than one failure modes. In that case, it is worthwhile to place the occurrence condition of these failure modes in one plot to realize the best estimation. This plot is termed here as the failure mode map. In this research excessive seismic loading is taken into consideration. Seismic load can induce several different types of failures.

1-2Seismic PRA

Many internal events can destabilize the nuclear power plant that causing accidents. In the case of internally caused initiating events efforts can be made to reduce the occurrence of such events. However, with regard to the externally caused initiating events like earthquake, it is nearly impossible to resist these initiating events. In addition, it is difficult to predict the occurrence of earthquake, and upon occurrence, the entire components within a nuclear power plant would be affected[18]. Therefore it is necessary to consider the safety issues in such a way that possible big earthquake would make no big threat to the nuclear power plant safety.

Seismic analysis and design of nuclear power plant facilities are performed according to pertinent codes and specifications. For example, nuclear power plants structures are designed by using the various standards developed by ASME [19], ACI [20], AISC [21], etc. and the national regulatory body's requirement which are mainly followed by the common rule provided by

international safety requirements like IAEA [22]. These specifications are usually following a deterministic approach[23][24]. In order to assure the safety of structures, margin of safety or conservatism is incorporated in each design step. These design guides generally make the plant safe; however, the margin of safety or the total conservatism during the service lives of nuclear facilities is not explicitly quantified [25]. The structural resistance due to seismic load is a function of many variables such as the magnitude of earthquake, duration, frequency as well as the material strength and geometry of the structure. Many of these variables are random and put statistical variations. In order to take the randomness and uncertainty in loads and structural resistance, etc. into consideration in the risk assessment, a probabilistic approach is chosen into consideration which is known as seismic probabilistic risk assessment (PRA). The objective of performing seismic PRA is to estimate the probability of core melt and radioactive release from a nuclear plant due to earthquakes. The major tasks which are done to perform the seismic PRA evaluations are described in following paragraphs.

1-2-1 Seismic hazard analysis

The seismic hazard at a power plant site is described by a hazard curve, a plot of the probability of exceedance vs. the peak ground acceleration. The major elements of the seismic hazard analysis include: 1. Identification of the seismicity and sources of earthquakes, such as source zone and active faults; 2. Assessment of the expected occurrence rate of earthquakes with different magnitudes or epi-central intensities using either seismicity data or geological studies; 3. Development of attenuation relationships; 4. Evaluation of local ground response. All the above information is integrated to generate the annual probability that the selected peak ground acceleration would be exceeded[26][27]. A complete seismic hazard analysis should also establish

the characteristics of ground motions as well as a hazard curve. The earthquake ground motion can be represented by a response spectrum, a power spectrum or a set of time histories[28]. The peak ground acceleration characteristics are generally selected by the history of seismic activity occurred on the specific site and engineering judgement. A typical hazard curve is shown in Fig 1-2.

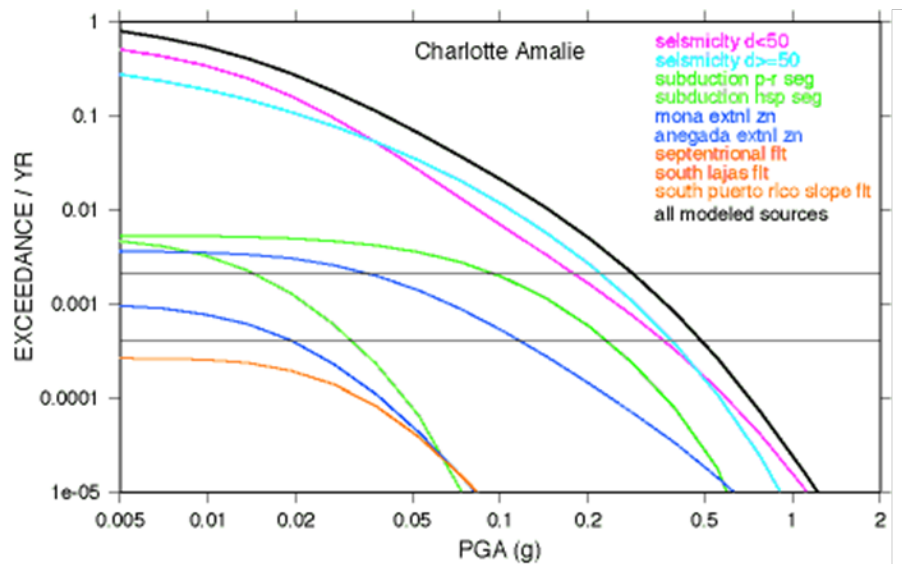


Figure 1-2 Typical seismic hazard curve [30]

1-2-2 Components and piping fragility assessment

The fragility of a structure or equipment is defined as the conditional probability of failure for a given value of a parameter [29]. The majority of seismic PRA's performed used peak ground acceleration (PGA) as the parameter. If the peak ground acceleration is used as the parameter, the response analysis is included in the fragility evaluation. The assessment of component (structure or equipment) fragility is a crucial task in a seismic PRA study. Accident sequences can be triggered by the occurrence of a severe earthquake. Fragility data determine how hard it is to pull this trigger. If the fragility data are overestimated or underestimated, the results of the accident

analysis will be distorted and subsequently mislead the analysis. So, it is very important to know the exact fragility of the structure or equipment. The fragility data are comes from actual earthquake experience or from experimental test. When the earthquake and test data do not provide sufficient information, simplified or advanced analytical model may be used to predict failure of structure or components. The analytically or numerically constructed fragility curves (which is eventually the failure curves) should be verified with experimental or actual earthquake data. However, the randomness and uncertainty may make the result very sensitive, so engineering judgement may necessary to make a fragility curve. A typical fragility curve is shown in Fig. 1-3.

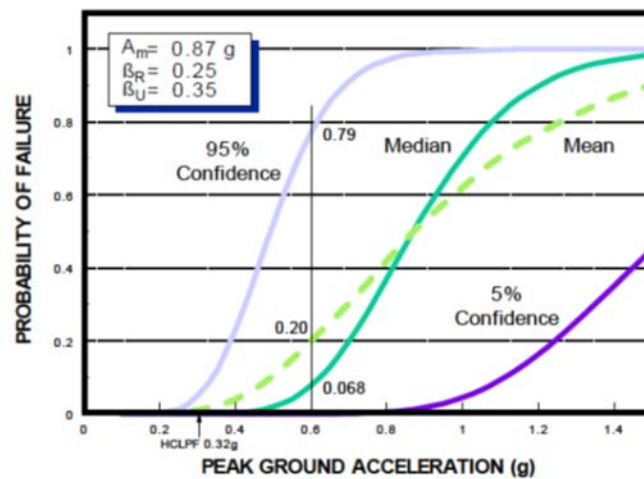


Figure 1-3 Typical fragility curve [32]

1-2-3 Accident sequence analysis and risk evaluation

When an earthquake occurs, a nuclear power plant may have a transient due to a loss of its off-side power or a large loss of cooling accident (LOCA). Such an event induced by an earthquake is known as initiating event and it can trigger a sequence of other events which involve various plant systems designed for responding to the initiating event. Thus, for each initiating event, an event tree can be developed which can postulate all possible accident sequence resulting from an

initiating event. An accident sequence may stop by successful use of mitigation through safety systems. The success or failure of a system usually depends on the interrelationship and redundancies between many components. The unavailability of a system is represented by a fault tree. So by using the event and fault tree it can be calculated the probability of core melt. Then, the core melt probabilities are used in the containment failure analysis to determine the probability of radioactive release to the environment.

Consequence analysis provides the final link in the PRA calculations and is intended to assess the effect to accidental releases of radioactivity on the environment. The probabilities of release of radioactivity are combined with the site model. Which includes weather data, population distribution etc., to obtain the probability of various adverse impacts[29].

For PRA studies, the failure may be defined by component capacity or functional requirements. A component usually has many possible failure modes, such as, a structure may fail due to cracking, yielding, crushing, and buckling and so on. The purpose of fragility assessment of a component is to predict how and where a component will fail and with what probability. So it is essential for the designer to know to clearly the exact failure modes for each component. Otherwise it is impossible to determine the capacity of a component, to choose a method for response analysis and to compare the results from different analyses of the same component. Identification of failure modes is also very important for collection of experimental; data. If failure modes are not well defined, we may use irrelevant data for fragility evaluation resulting in erroneous calculations.

1-3 Characteristics of seismic load

There are various types of load acting in nuclear power plant includes internal pressure, dead weight, thermal load, seismic load etc. These loads possess different characteristics and therefore have specific effects on failure of components and piping [9]. There are mainly two types of loading depending on the stress-strain response produced by the load, such as, load-controlled and displacement-controlled types of loading. In a structure, the main stress induced by an external force is called primary stress. For example, the stress generated in a beam with one fixed and a weight is placed at the other end. In an elastic-perfectly plastic body, once the primary stress reaches the yield stress of the material, plastic deformation continues to grow indefinitely, which means that plastic instability occurs without the additional external force. An example of such primary stress would be the hoop stress in a cylindrical vessel subjected to internal pressure, or the example we provided earlier. In either case the deformation increases without any increase of the external load. On the other hand, a secondary stress is a type of stress generated in a structure which meets the compatibility condition of deformation. For instant, the stress induced in a bar with one end fixed and a certain amount of forced displacement applied to the other end. In this case, the plastic deformation may appear if the stress is exceeding yielding stress but structure does not grow indefinitely unless the external force is increases. Thermal stress is one of the practical examples of this type of loading. Secondary stress is also called self-controlled stress. According to the characteristics, the primary stress is load-controlled stress and secondary stress is displacement-controlled stress. These two types of stress have different effects on structural integrity. Figure 1-4 compares the behavior of load-controlled and displacement-controlled loadings, in the case where loads are applied to a bar to achieve the same amount of elastic deformation in both cases. It has been seen in the Fig. 1-4 that under load-controlled conditions,

the strain in the bar increases under constant stress and under displacement-controlled conditions, the load decreases under constant strain.

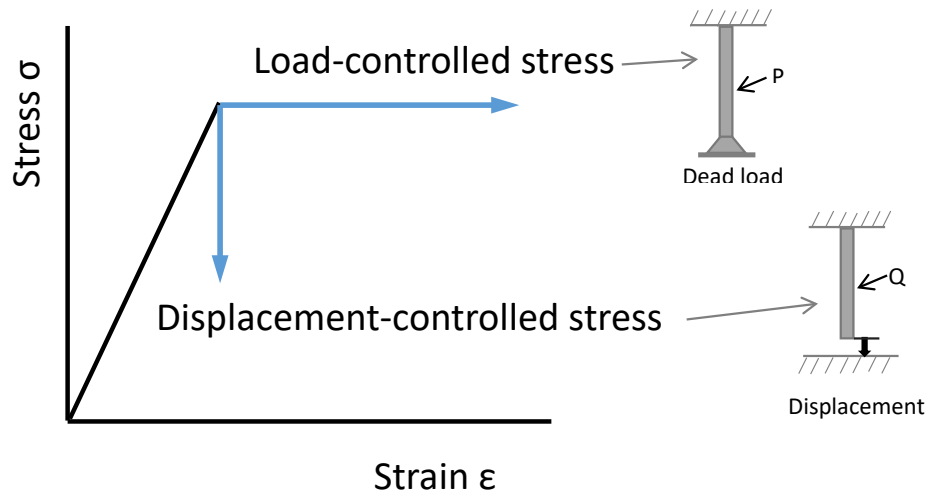


Figure 1-4 Difference of characteristics of load-controlled and displacement-controlled loading [9]

Seismic loading conventionally considered as load-controlled loading. But recent studies have also found the displacement-controlled characteristics of seismic loading. Seismic PRA is focused on only peak ground acceleration and in this case it is considered as load-controlled load. On the other hand, seismic load is alternate one and when the structure and component is shaking due to earthquake, the structure has its own dynamic response. So, the characteristics of seismic load, whether it is load-controlled or displacement-controlled still have an ambiguity.

1-4 Failure modes under seismic loadings

Seismic load can cause several different failure modes in nuclear power plant's structure and component. Fatigue is one of the well-known failure modes for such dynamic

load[30][31][32][33][34][35][36][37][38][39]. But other failure modes as ratcheting deformation or collapse can also occur depending on loading conditions [16][40][41][42][43][44][45].

1-4-1 EPRI piping and fitting dynamic reliability tests[40]

The component test program is focused on the dynamic behavior and failure mode of typical pressurized piping components including elbows, tees, reducers, nozzles and weld attachments. The test specimens consists of both carbon steel and stainless steel 6 inch diameter components with various thickness and internal pressures. The dynamic load had various frequency started from low frequency to high frequency. For seismic test a shaking table was used to produce desired input acceleration. The emphasis of the test program has been placed on seismic overload. The specimen was attached to a specially-designed shaker-sled fixture at one end and to an extended inertia arm at the other end. A typical setup for in-plane elbow test is shown in Fig. 1-5. During the test, a shaker-sled was driven by a group of four 1000 lb hydraulic actuators which would produce up to 20g input base motion accelerations to the system, and the inertia arm reacted to the vibratory base motion which in turn induces severe cyclic inertia loading to the test component. A 20-s amplified prototypical plant floor seismic time history, as shown in Fig. 1-6, was selected as the input driving force. The high amplitude input was repeated until the failure occurs. The peak frequency of the input acceleration was set in such a way that the structure always gets maximum response. Generally the input frequency was set slightly lower than the natural frequency of the test specimen. Total 32 channels of instrumentation was attached to the specimen. These includes accelerometers, displacement sensors, pressure meters and strain gages to measure the response as well as the applied moments and forces during the test. To check crack on the specimen between the tests, non-destructive tests was carried out as well. The input of seismic test

was increased typically 15 to 25 times than the typically calculated design limit level D stress were needed to cause rupture.

The experimental results were analyzed and found that fatigue ratcheting was the dominant failure mode for pressurized piping components, and low-cycle fatigue or ratcheting buckling (which is defined as collapse in our research) due to gravity effect has been failure mode for those unpressurized components. All the pressurized components experienced significant swelling due to ratcheting, this swelling caused wall thinning and eventually developed cracks.

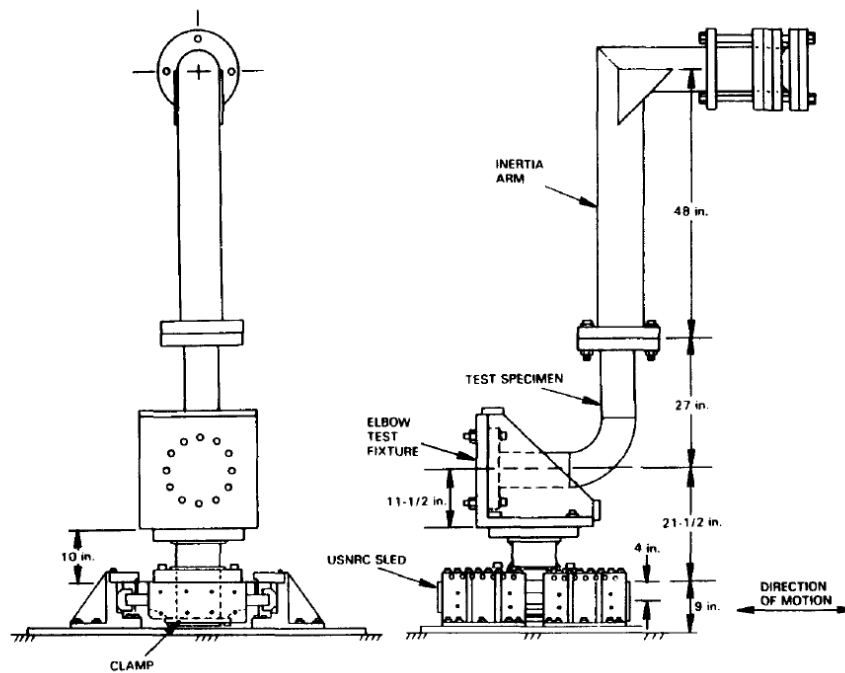


Figure 1-5 In-plane elbow test setup[40]

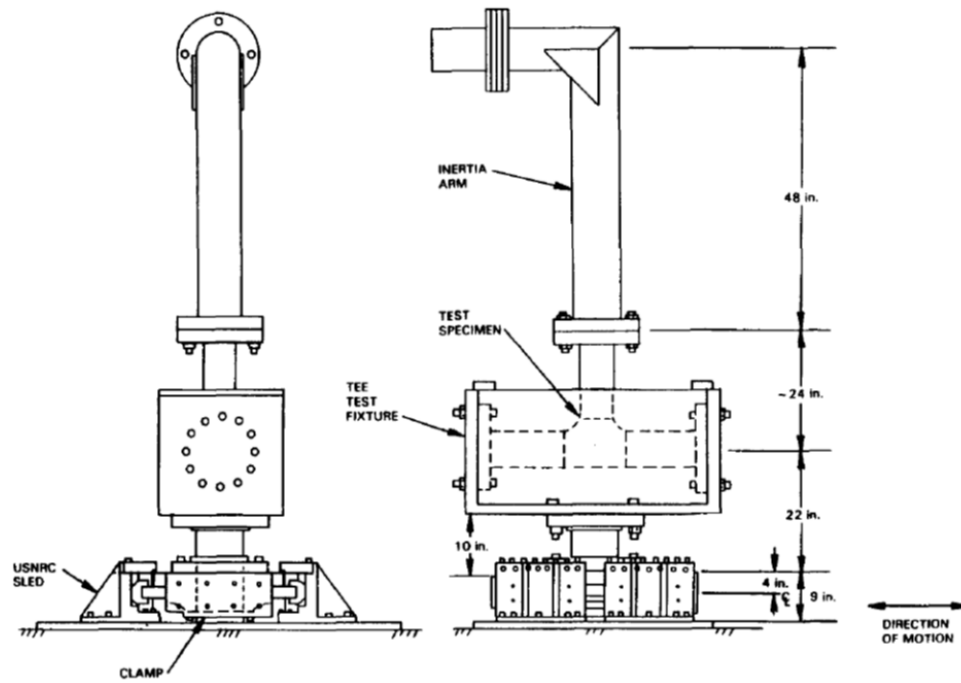


Figure 1-6 In-plane tee test setup [40]

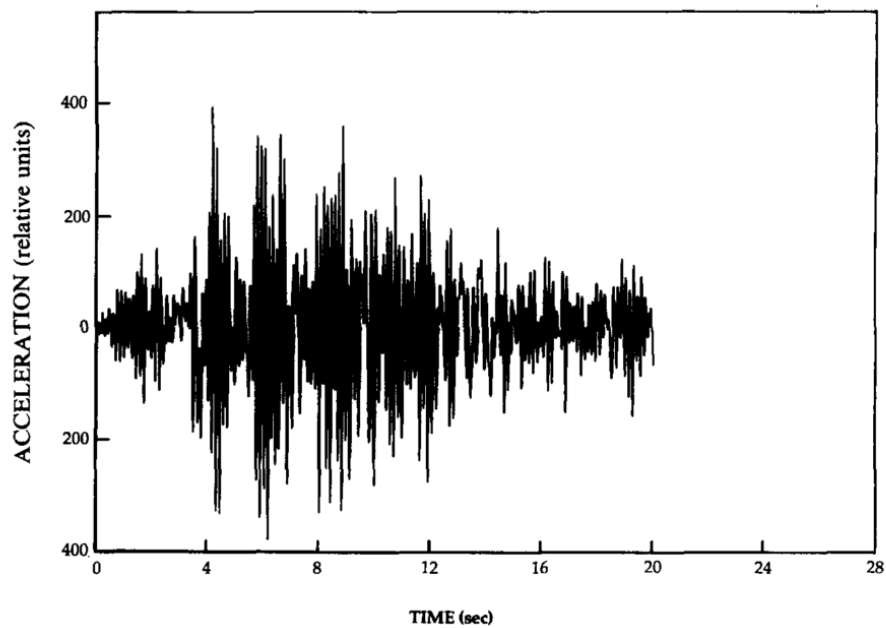


Figure 1-7 Input seismic motion time history[40]

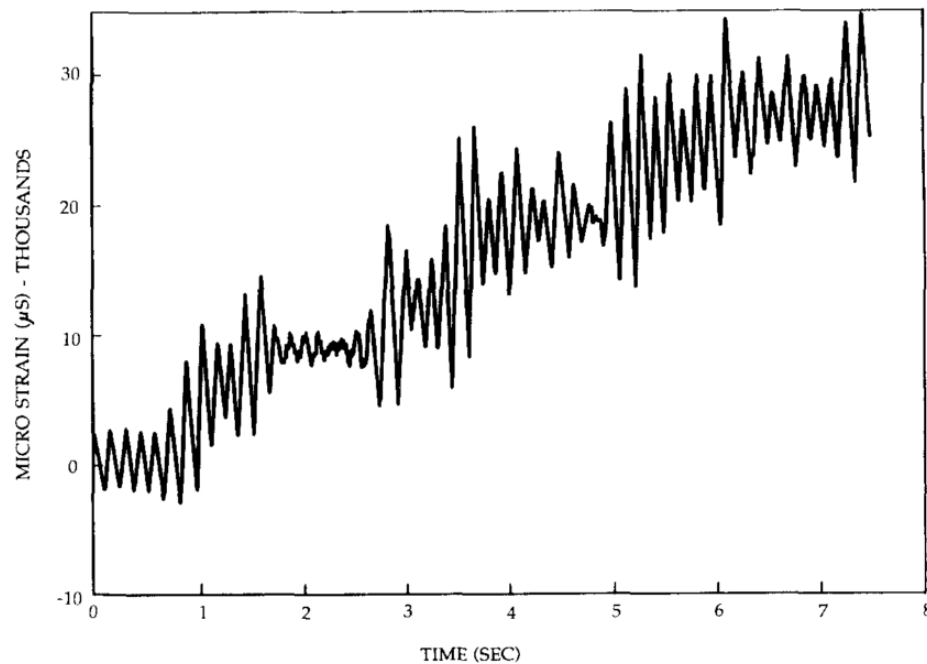


Figure 1-8 Input strain time history showing ratcheting behavior [40]

1-4-2 Large scale piping system tests[43][46][47][48]

The objectives of piping tests were to clarify the elastic-plastic response and ultimate strength of nuclear piping and to ascertain the seismic safety margin of the seismic design code. Prepare new analytical tools for elastic-plastic response analysis and evaluate a fatigue damage criteria was also another objective of this piping tests. In this project piping component tests, simplified piping system tests and large-scale piping test were conducted. Piping component tests were included elbow, tee, reduced etc, whereas 2 models of simplified piping system were tested. Experiments for two models of large scale piping system were also performed. Different types of loading conditions were performed which includes quasi-static cyclic loading under sinusoidal deflection control, the dynamic cyclic loading under inertial force due to seismic excitation and sinusoidal excitation. For simplified piping systems and the large scale piping systems, seismic

excitation tests were done using shaking table. A postulated seismic motion on the floor of a reactor building was applied to the shaking table (Fig. 1-8). Piping system tests, it was observed that the resonant frequency was decreased and damping ratio was increased when the excitation level was increased. The figure of elbow specimen test and large scale piping system tests were shown in Fig. 1-9 and 1-10 respectively.

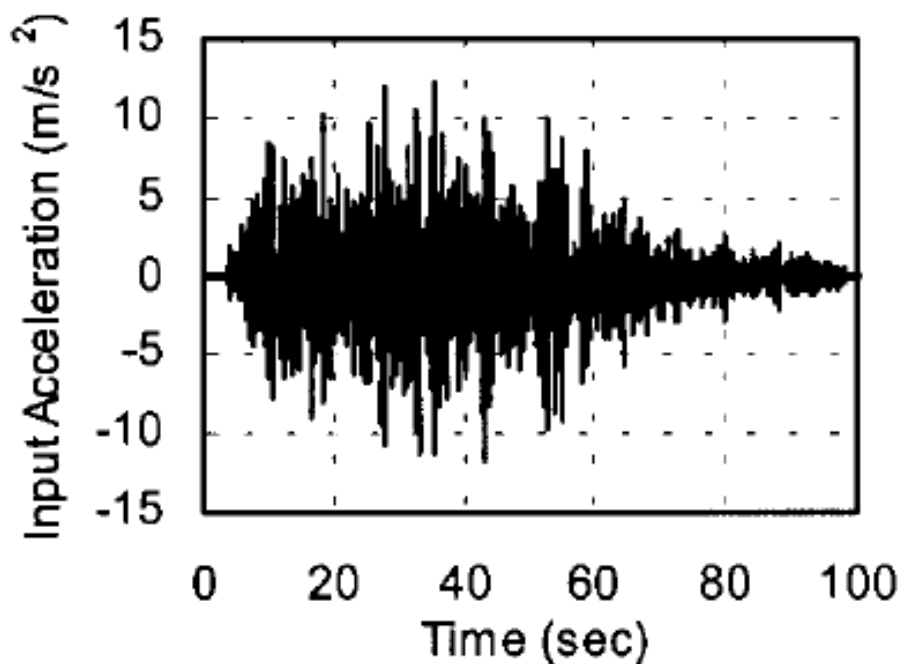


Figure 1-9 Time history of seismic input wave [48]

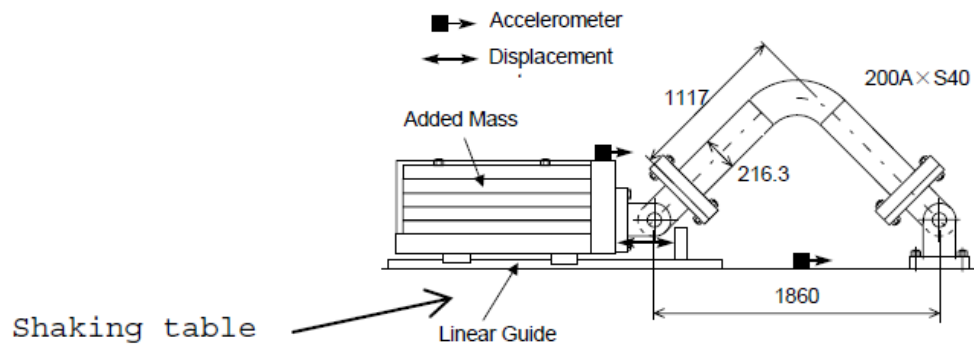


Figure 1-10 Elbow specimen for dynamic tests [43]



Figure 1-11 Large scale piping system model [43]

The results of this test were similar to EPRI piping and fitting dynamic reliability tests. The major failure mode in this case is also low cycle fatigue with ratcheting. It was also clarified that the fatigue life of piping components were about 1/5 times of the parent metals for carbon steel and 1/2 times for stainless steel for same strain range. One of the reasons to decrease the fatigue life

is due to the presence of ratcheting. For the large scale piping system the low cycle fatigue was observed at the elbow where the largest strain was forecasted. The typical hoop strain fatigue lives of components with its parent metals life is shown in Fig 1-11.

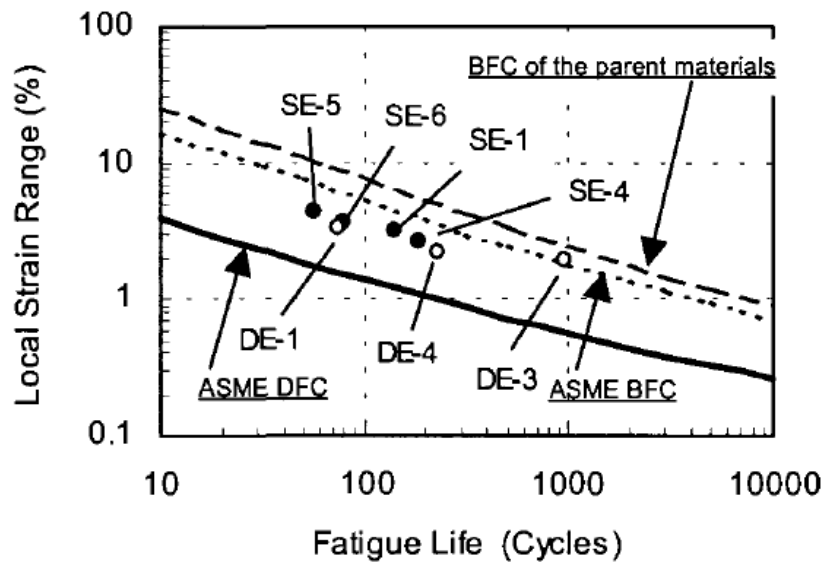


Figure 1-12 Fatigue lives through the piping component tests [48]

1-4-3 Trial model tests of pipes under excessive seismic loads[44]

The objective of these experiments was to clarify the dominant failure modes of pipes under very high seismic motions, especially ratcheting and collapse. Lead (Pb) pipes have been tested on shaking table. The material used in this study was Lead (Pb) because the experimental studies with steel pipe are difficult to achieve, mainly due to the limitations of testing facilities and safety concern. The excitation tests were conducted to observe failure modes other than fatigue failure in pipe structures. Two types of arrangements have been tested for the elbow pipe specimen configuration in this experimental study. Inverted type specimen and pendant weight type specimen. In inverted type elbow specimen configuration additional mass was added to the upper

part of the specimen shown in Fig 1-12. Another type of that suspended the additional mass was used in addition to the inverted type specimen to investigate the effect of gravity on the failure process. This type of specimen is referred as pendant-weight type specimen. Pendant-weight type specimen is shown in Fig 1-13.

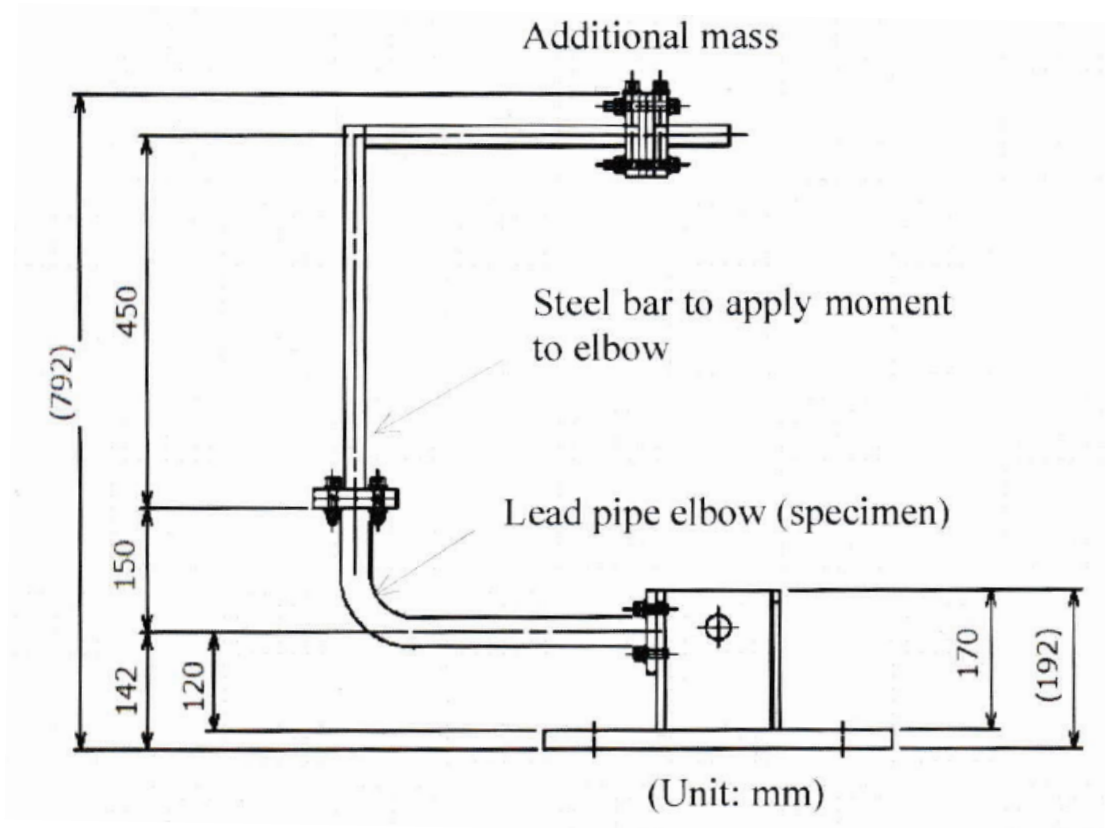


Figure 1-13 Inverted type specimen [44]

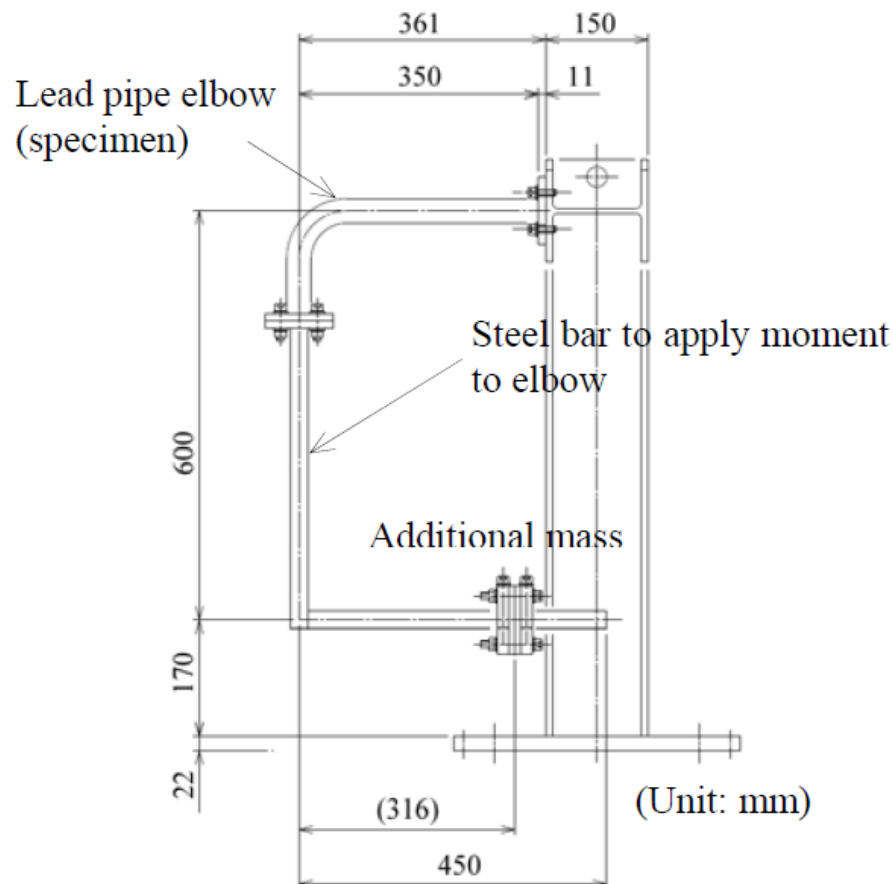


Figure 1-14 Pendant-weight type specimen [44]

The input waveforms were mainly sinusoidal with tapered at the beginning and end of the steady amplitude portion. There was various numbers of cycles of the steady wave, generally started from 1 to 20 waves. The frequency of the input wave was changed according to the purpose of the excitation. Except of sinusoidal wave, some modified seismic wave was also put as input wave. The modified sinusoidal wave was made from actual seismic wave recoded in the 1995 Kobe earthquake. The modified input seismic had half the time span of the actual wave and amplifying the maximum acceleration to twice that of original seismic motion. Typical inputs waves are shown in Fig 1-14 and Fig 1-15.

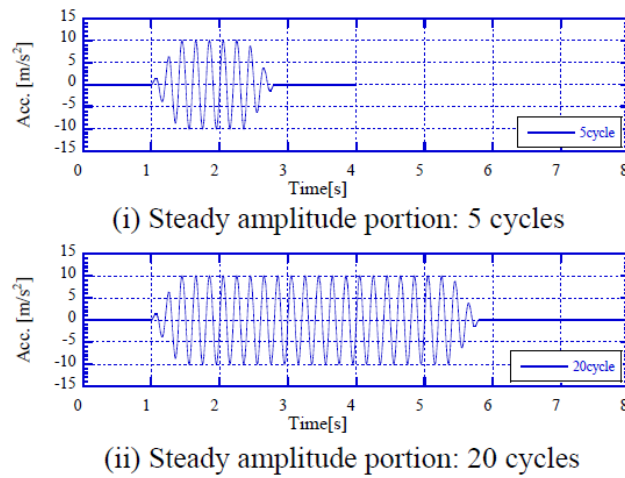


Figure 1-15 Sinusoidal waves with tapered part [44]

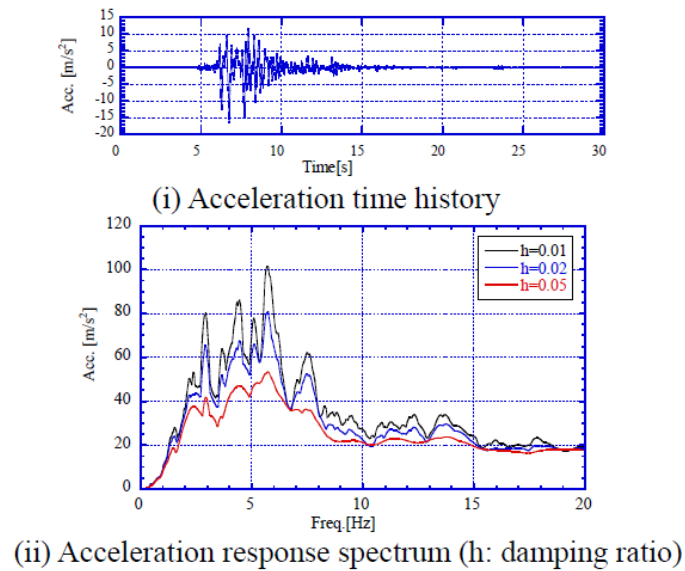


Figure 1-16 Input seismic wave [44]

The tests were conducted in 2014 and 2015. The occurrence conditions of failure and different failure modes were identified by changing the additional mass and input acceleration with frequencies. Depending on the specimen configuration, two types of failure modes was observed. For inverted type specimens, deformation accumulated in the elbow-closing direction and finally collapse occurs. This type of failure is termed as ‘ratchet-collapse’. Figure 1-16 shows the process

of this type of failure mode. Another type of failure mode was detected in pendant-weight type specimen, where the failure mode was overall deformation of the entire pipe. Peeling and cracking of paint were observed at the elbow and anchor. Figure 1-17 shows this type of failure. From the above discussion it can be said that the observed failure modes from this experimental studies were ratcheting and collapse.



Figure 1-17 Progress of ratchet collapse failure mode observed in the inverted type specimen

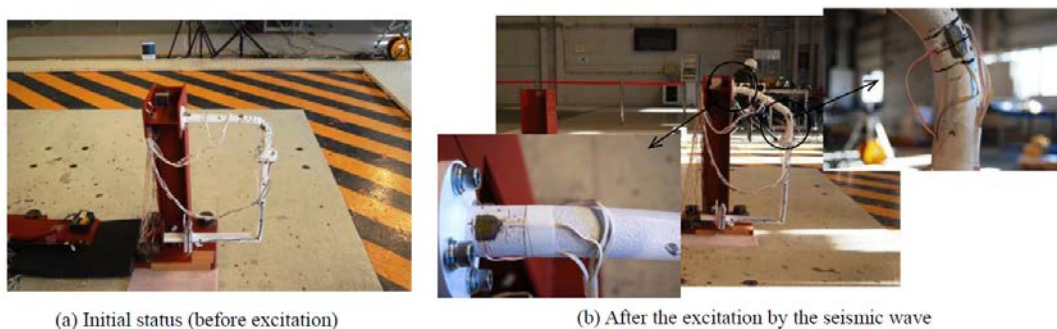


Figure 1-18 Failure mode observed in the pendant-weight type specimen

1-4-4 Fundamental experimental studies under seismic loading[16]

Fundamental vibration test have been carried out in our laboratory to clarify the probable failure modes. To clarify unclear failure mechanisms, authors have planned step by step experimental studies on failure mechanism for excessive seismic loads. The experiments have been

conducted on plate shaped specimens made of Pb and Pb-Sb alloys. Some specimens were with notch and others without. Vibrations which were given as a simulated seismic load had two different shapes. One was sudden acceleration for understanding the effects of maximum peak acceleration. Another type of vibration was continuous sinusoidal wave to investigate the effect of loading cycle. The frequency of the input acceleration was similar to the natural frequency of the model. The idea of the possible failure modes and input loadings are shown in Fig 1-18 and Fig 1-19 respectively.

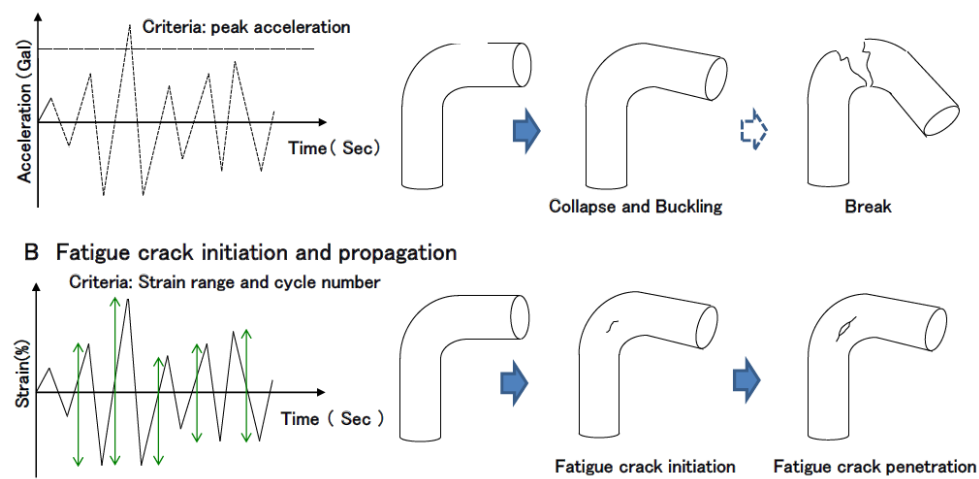


Figure 1-19 Possible failure modes under extreme seismic load

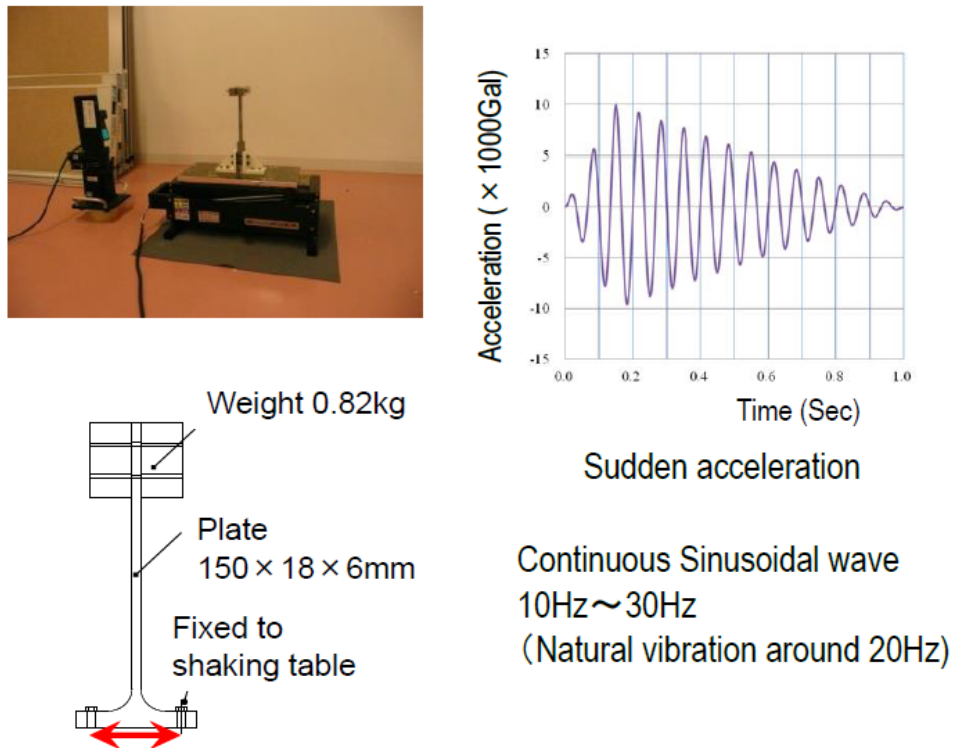


Figure 1-20 Fundamental vibration test experimental setup

The results of these tests were following –

Collapse: Pb100% specimen without notch subjected to sudden acceleration,

Brittle fracture: Pb80% – Sb20% specimen with notch subjected to sudden acceleration

Fatigue failure: All other conditions.

The figures of the failed cases are shown in Fig 1-21.



Figure 1-21 Obtained Failure modes from fundamental vibration strength tests

1-4-5 Probable failure modes due to seismic loading

Above mentioned literatures concluded that fatigue is one of the major failure modes for the pipe components especially when the pipes are pressurized. Apart from fatigue, ratcheting is one of the most common failure modes due to seismic loading. And excessive ratcheting leads the structure to collapse. Some real seismic events also showed the similar phenomena of failure on structures. In 1994 Northridge earthquake caused collapse of a large-diameter flexible corrugated metal pipe [49]. One year later Daikai subway station collapsed in Kobe, Japan due to Hyogoken-Nanbu (Kobe) earthquake [50]. So the conclusion of literature is that, the probable failure modes due to seismic loading are ratcheting, collapse and fatigue. These failure modes are occurring depends on the loading and geometry of the structure.

1-5 Objectives of the present study

Excessive seismic loading is one of the extreme loading categorized as DEC. From the structural point of view, the preparation for DEC is somewhat difference from conservative approach for design. DEC requires best estimate strength evaluation of components and piping of nuclear power plants. For the best estimate approach, it is necessary to clarify the dominant failure

modes due to extreme loading. Clarification of dominant failure modes includes the identification of probable failure modes as well as the occurrence conditions of these failure modes. The possible failure modes due to seismic loading are ratcheting, collapse and fatigue as discussed in Section 1-4-4.

Apart from these, it has been discussed in Section 1-3 that the characteristic of seismic load is ambiguous. Clarification of seismic loading characteristics with frequency effects on failure modes is the first half objective.

To realize and understand the effect of various loading on several different failure modes, it is worthwhile to put the occurrence conditions of different failure modes in a same plot which is defined as the failure mode map in this research.

First, to clarify the failure modes, beam shaped model is analyzed by dynamic inelastic finite element method. Then results of beam analyses are verified by dynamic experimental analyses in the laboratory. After validation the dynamic inelastic finite element scheme is extended to elbow pipe model.

In this present study, to propose a failure mode map due to seismic loading is the latter half objective. To make failure mode map the clarification of different failure modes are needed. So, to clarify the ratcheting failure mode for beam shaped model and elbow pipe model is one of the specific objective of this study. Similar to ratcheting, other failure modes such as collapse and fatigue are studied and plotted on the same failure mode map.

The results from these analyses were placed on the non-dimensional primary and secondary stress parameter graph similar to Bree diagram. Finally the authors proposed a failure mode map under seismic loading.

1-6 Outline of the thesis

In this thesis, the main contents in the subsequent chapters are as follows.

In **Chapter 2**, the methodology of this study is discussed. Methodology section includes the different approaches used in this study including finite element approach and experimental approach. Also the different types of models used in this study namely beam models and elbow pipe models are presented and different types of loading on these modes are described.

In **Chapter 3**, results of ratcheting failure mode for beam model and elbow pipe model is discussed. This chapter started by explaining the various theories of ratcheting along with the theoretical results of this specific type of ratcheting. The discussion of FEA results and experimental results are also presented in this chapter. Finally the clarification of characteristics of seismic results is explained.

In **Chapter 4**, other failure modes analyses are shown. This chapter started with collapse results for beam model by FEA. Then validations of beam model results are shown. Collapse results for elbow pipe model are also presented for FEA. The first stage experimental results of fatigue experiments are also presented.

Chapter 5 presents the proposal of failure mode map for ratcheting, collapse and in some cases fatigue for both FEA and experimental cases.

Finally, the conclusions and some suggestions for future work are presented in **Chapter**

Chapter 2 - Methodology

Both experimental and analytical approaches have been carried out to clarify the occurrence of different failure modes. Two types of models have been analyzed for finite element method, namely- beam model and elbow pipe model. Furthermore, to validate the finite element scheme experimental analysis was also carried out. Experimental analyses were accomplished for beam model. Some experiments for elbow model were also observed and made similar geometry model for numerical model. Here in this chapter the details of the geometry, material and loading conditions of different models are discussed.

2-1 Analytical approach with finite element method

Two different finite element models are analyzing for different geometries. The modelling is done by FEMAP[51] software and then the finite element analyses are done by FINAS/STAR code[52]. The two different models are – beam model for understanding of basic mechanisms and elbow pipe model for validation of applicability to piping.

2-1-1 Beam model for understanding of basic mechanisms

For the beam analyses, a rectangular beam with a cross-section of 6 X 13 mm was used. The length of the beam was 140 mm. The model is shown in Fig. 2-1. The element type was chosen plane stress to get more integration point than by simple beam element. The plane stress element (QUAD4) is a two-dimensional isoparametric plane-stress element which uses Lagrangian two-dimensional linear interpolating equation for its displacement function. In calculating the element stiffness matrix, its vertical component of stiffness is calculated by Gauss' numerical integration

of 2X2 point, and its shear component of stiffness is calculated by central integral method. The brief summary of 'PlaneStress (Quad4)' element is given in the Table 2.

Since the geometry is simple and loading was bending, a simple rectangular mesh was constructed. The mesh around the base of the beam was very fine as it is high stress region and mesh is relatively coarse near the free end of the beam as the stress and strain of this region is insignificant for the calculation. Meshed model is shown in Fig. 2-2. Total number of mesh was 3840.

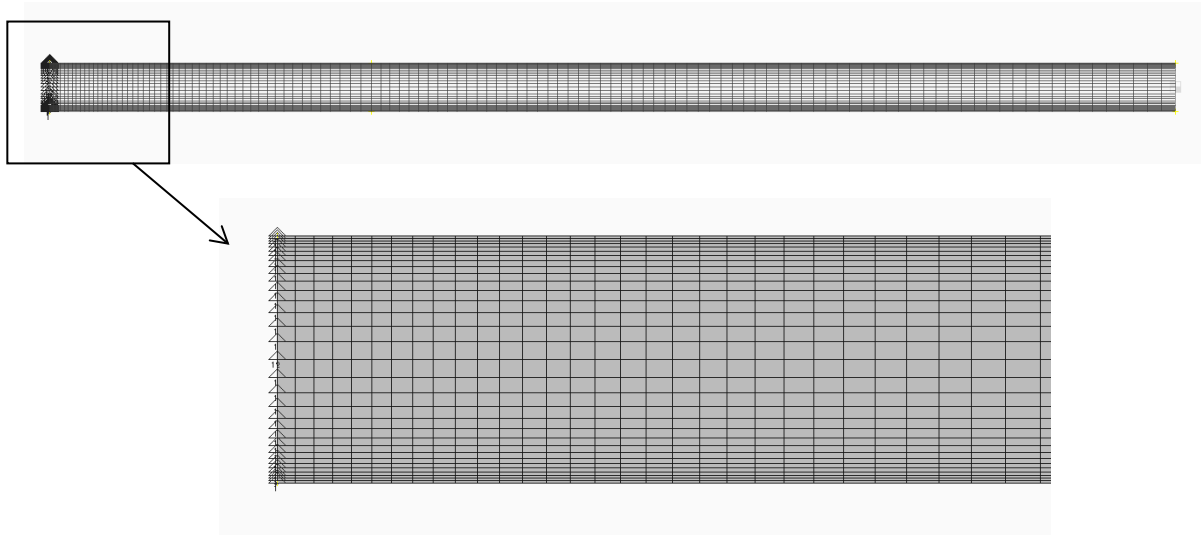


Figure 2-1 Meshes of the beam model

Table 2-1 Geometry of the beam model

Geometry (Dimensions)		
Length (mm)	Thickness (mm)	Width (mm)
140	6	13

Table 2-2 The summary of Element type " PlaseStress (Quad 4)' [54]

Shape	Two-dimensional quadrilateral plane element
Number of nodes	4
Nodal coordinates	X, Y coordinates
Nodal degree of freedom	Degree of freedom number 1= u_x , 2= u_y
Displacement function	Lagrange two-dimensional linear interpolating equation
Integration point	5 (2X2 and centroid)
Stress component	σ_x , σ_y , τ_{xy}
Strain component	ϵ_x , ϵ_y , γ_{xy}
Geometrical shape	Plate thickness t

2-1-2 Material properties of beam

The elastic-plastic material properties were chosen to approximate those of pure Lead (Pb) at room temperature. The choice of material was based on experimental conditions. Due to the limitation of laboratory facilities, it was difficult to accomplish failure with specimen made of steel. On the other hand, the stress strain characteristic of steel has similarity with lead, so for experiments it was used lead or lead alloy. An elastic-perfectly-plastic material, having a Poisson's ratio, ν , of 0.44, was used. The material properties used are given in Table 2-2.

Table 2-3 Material data for elastic plastic analysis of beam

Material	Lead (Pb)
Young's Modulus, E	16 GPa
Yield stress, S_y	5 MPa
Poisson's ratio, ν	0.44
Density, ρ	11340 kg/m ³

The Von-Mises effective stress criterion was used to relate the multi-axial behaviour to uniaxial behaviour for elastic-perfectly-plastic cases. The most commonly used model for elastic plastic analysis is the elastic-perfectly-plastic model. The model assumes that there is no hardening at all. The model will predict an indefinite plastic strain whenever the applied stress is above the yield stress. For strain controlled cycling, the model cannot describe hardening or softening, shown in Fig. 2-2. Though it is simple and doesnot usually describe real material model behaviour accurately, the model can be used to accurately predict the load bearing capacity of some simple structures[53][54]. This model can analyze the mechanism of ratcheting for various simple stress components [55]. Elastic-perfectly-plastic was used for Bree diagram for ratchet boundary as well. Various sophisticated material modellings are developed for ratcheting strain prediction but none of these are accurately presdict the ratchet srtain for various loading conditions and geometry. Furthermore to compare the result with theoritical ratchet model, it was better to use elastic-perfectly-plastic material model.

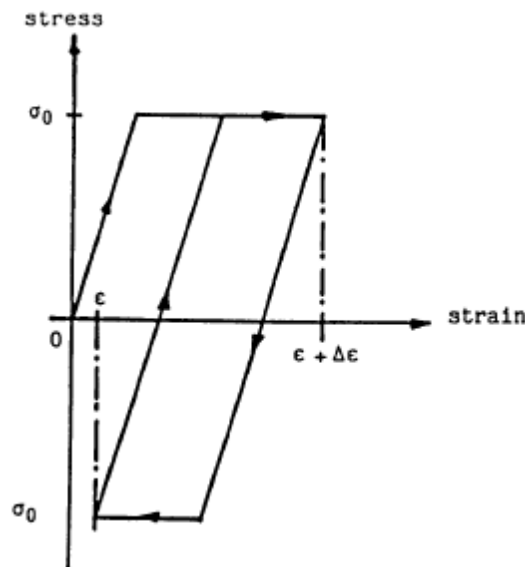


Figure 2-2 Elastic-perfectly-plastic material model [57]

2-1-3 Loading and analysis conditions of beam

There are two types of loadings were applied to the beam model. Gravity loading was applied by two ways- one was by the additional mass put at the free end of the beam and another was the self-weight of the beam. The additional mass which was placed at the free end of the beam has been varied throughout the finite element analysis to get various load combination. The additional mass is termed as ‘NodeMasses’ in FENAS/STAR code. The ‘NodeMasses’ data defines the masses to be directly added to the degree of freedom of nodes.

The gravity load was act as primary load whereas to get ratcheting a secondary load was needed. In this case, a cyclic acceleration at the base of the beam was put. This base acceleration acted as the source of reversal dynamic loading which can be assumed as seismic loading. The shape of the acceleration wave was sinusoidal. Base acceleration was act as a pseudo secondary load. It is said to be pseudo, because it has been discussed in section 1-3 that the type of seismic

load has dual characteristics, so it was not sure whether it act as load-controlled or displacement-controlled. For each gravity load case, the input acceleration had been changing to get the occurrence condition of failure (ratcheting, collapse). The frequency of input acceleration was also varying to check the effect of frequency on failure occurrence. So in other words, the various combination of node mass and base acceleration with different frequencies made the occurrence of failure at various load combinations.

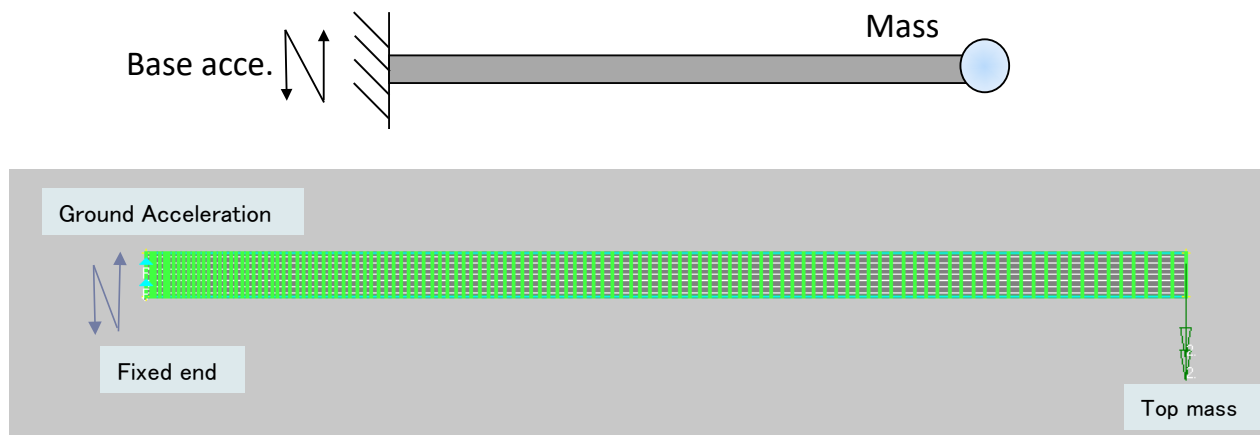


Figure 2-3 Loading and boundary condition of the beam model

The loading and boundary conditions of the beam model was shown in Fig. 2-3. As mentioned earlier, the base of the beam was fixed whereas all other nodes have degree of freedom in X, Y directions. The gravity force was put downward, and the acceleration was put at the base of the beam.

The analysis was done by dynamic elastic plastic finite element method. The large deformation was on. The damping type was used Rayleigh. The Rayleigh attenuation shown in equation (2-1) was used for the attenuation. With reference to the attenuation ratio of 2% obtained in the experiment, the coefficients were adjusted so that the attenuation ratio was 2% for each input frequency.

$$[C] = \alpha[M] + \beta[K] \quad 4 - 1$$

Where $[C]$ is the attenuation matrix, $[M]$ is the mass matrix, and $[K]$ is the stiffness matrix. The method of determining the coefficient is represented by the following with respect to the target frequency range.

$$\alpha = \frac{2\omega_1\omega_2(\zeta_1\omega_2 - \zeta_2\omega_1)}{\omega_2^2 - \omega_1^2} \quad 4-2$$

$$\beta = \frac{2(\zeta_2\omega_2 - \zeta_1\omega_1)}{\omega_2^2 - \omega_1^2} \quad 4-3$$

Here, ω_1 = natural frequency for the first mode; ω_2 = natural frequency for the second mode; ζ_1 = damping ratio for the first mode; ζ_2 = damping ratio for the second mode
 ω_1 and ω_2 is coming from the experiment, whereas the value of ζ_1 and ζ_2 is choosing in such a way that will satisfy the equation (4-1) and give a satisfactory damping value.

2-1-4 Elbow pipe model for applicability validation of applicability to piping

For elbow pipe model, a pipe with outside diameter of 33 mm with an outside diameter to thickness ratio of 11 was used. The geometry was similar to the experimental model mentioned in [44]. The geometries and dimensions of the model are shown in Fig. 2-4 and Table 2-4. The element type was used Shell(QUAD4) for the pipe section and Beam (LINE2) element was used for fixed unreformed parts.

The Shell(QUAD4) element is a three-dimensional four-node quadrilateral isoparametric shell element. Its displacement function is assumed to be a bilinear equation. This shell element is degenerated three-dimensional continuum element, and is applicable for both thick-walled and thin-walled structures. This element can be performed elastic analyses, inelastic analyses due to material nonlinearities such as plasticity and creep, and geometrically nonlinear analyses that takes

account of large deformation and large strain. It has total 45 integration points (5 points in plane and 9 points in plate thickness direction). The brief summary of ‘Shell(Quad4)’ element is given in the Table 2-5. Fine mesh was used for elbow pipe section especially in the bend region as the maximum strain was expected to occur in this region. The mesh size was optimized.

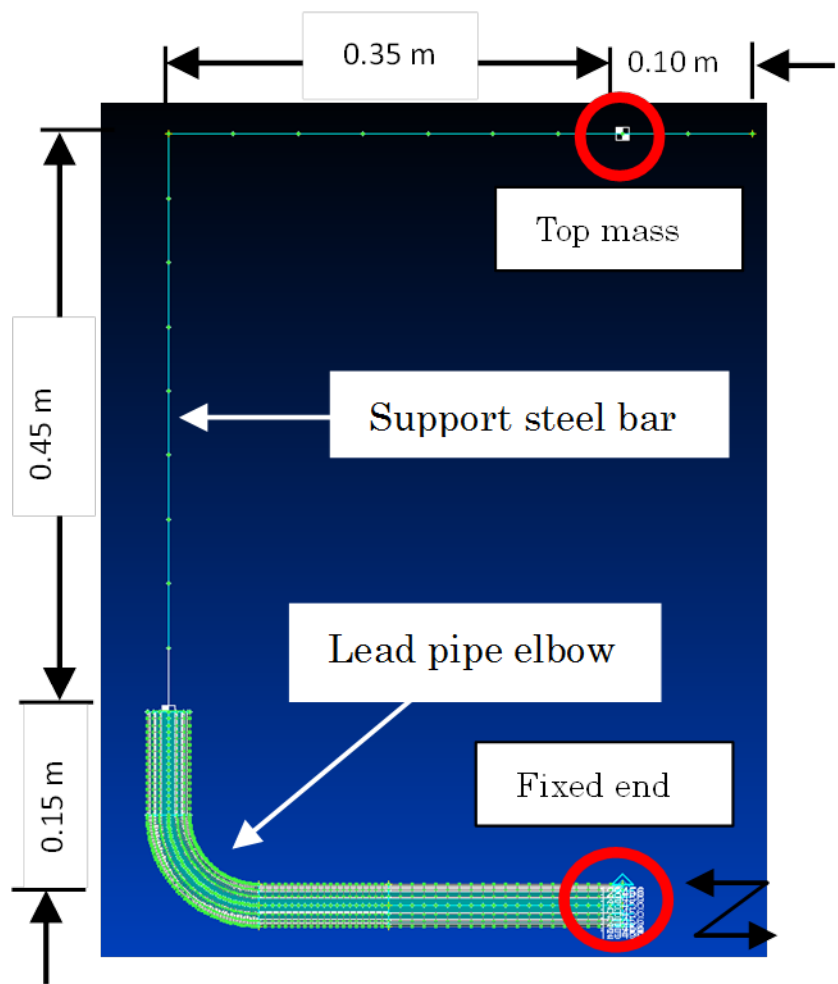

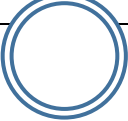


Figure 2-4 Geometry and dimensions of pipe

Table 2-4 Dimensions of elbow pipe and support beam

Support Beam	Elbow Pipe
	

Cross-section: (40X25) mm Thickness: 1.2 mm	Outside Dia.: 33 mm Inside Dia.: 30 mm
--	---

Table 2-5 Summary of element type 'Shell (Quad 4)' [54]

Shape	Two-dimensional quadrilateral plane element
Number of nodes	4
Nodal coordinates	X, Y, Z coordinates
Nodal degree of freedom	Degree of freedom number 1= u_x , 2= u_y , 3= u_z , 4= θ_x , 5= θ_y , 6= θ_z
Displacement function	Lagrange two-dimensional linear interpolating equation
Integration point	45 (5 points in-plane and 9 points in plate thickness direction)
Stress component	σ_x , σ_y , τ_{xy} , τ_{yz} , τ_{zx}
Strain component	ϵ_x , ϵ_y , γ_{xy} , γ_{yz} , γ_{zx}
Geometrical shape	Plate thickness t

2-1-5 Material properties of elbow pipe

Similar material has been used for elbow pipe as like beam material. The only difference which was taken into consideration in the case of elbow pipe material was bi-linear effect of plasticity. In the case of beam analyses elastic perfectly plastic material was used whereas for elbow pipe case a linear approximation up to the strain of 5% in the stress strain diagram of lead shown in Figure 2-5, the work hardening coefficient was set to 50 MPa and the kinematic

hardening rule was used. For support structure, stainless steel is taken as material. As there was no deformation allowed in the support structure, so only elastic properties was input.

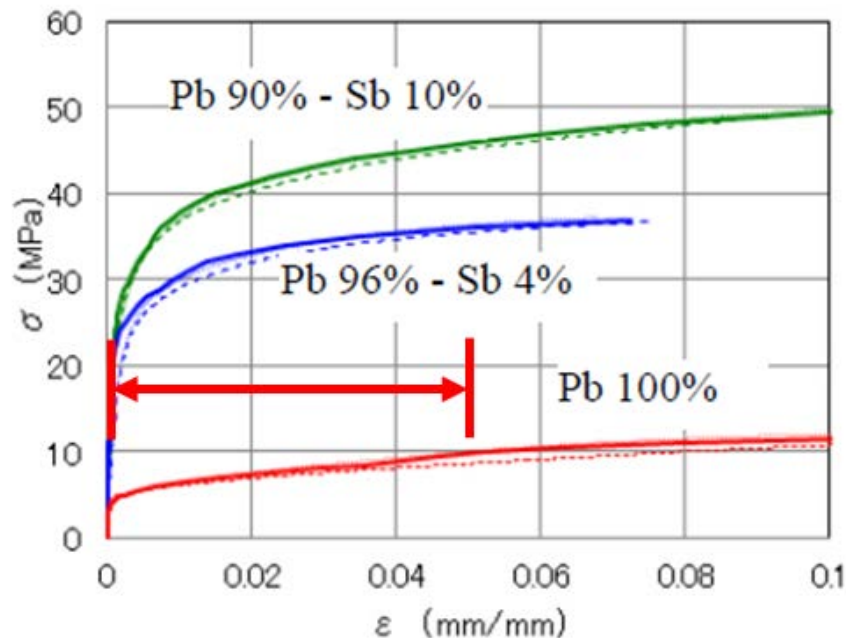


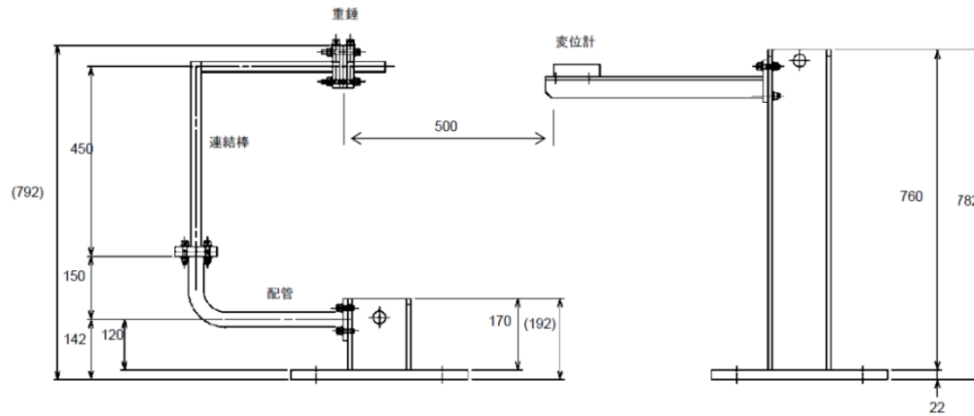
Figure 2-5 Pure lead stress strain diagram

2-1-6 Loading and analysis conditions of elbow pipe

Similar loading conditions were applied for elbow pipe case as for beam case. Two types of loading were applied, one was gravity loading and another one was inertia loading. Gravity loading was applied by putting an additional mass at the top of support bar and the self-weight of the support bar. The loading was analogous to the loading of experiment done by Nakamura et. al. []. Figure 2-6 shown the experimental setup of Trial model tests by Nakamura et. al.

There were three parameters which have been changed to get the occurrence conditions of failure. These three parameters were- steady bending stress due to gravity load, dynamic bending stress due to inertia load and the frequency of the input acceleration. The Steady bending stress has been changed by changing the additional weight. The dynamic bending stress could change by

changing the input acceleration. And the frequency was also changed for same acceleration to get the effect of frequency on occurrence of failure.



(a)

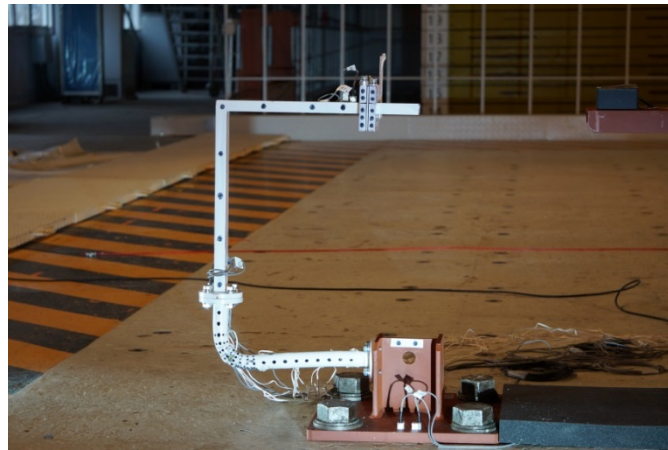


Figure 2-6 Trial model tests experimental setup (a) Dimensions and loading (b) Photograph of real experiment [46]

The dynamic elastic plastic finite element analyses were conducted as same as beam model. The base of the elbow pipe was fixed (showed in Fig 2-4) whereas all other nodes have degree of freedom in X, Y and Z directions. The gravity force was put downward, and the acceleration was put at the base of the elbow pipe.

2-2 Experimental approach

Experiments have been done for ratcheting, collapse and fatigue failure modes but only for beam models. Similar loading conditions have been trying to put in the case of experiment as like finite element analyses. The primary purpose of experimental analyses is to validate the finite element results. Figure 2-7 is showing the similarities between finite element setup and experimental setup.

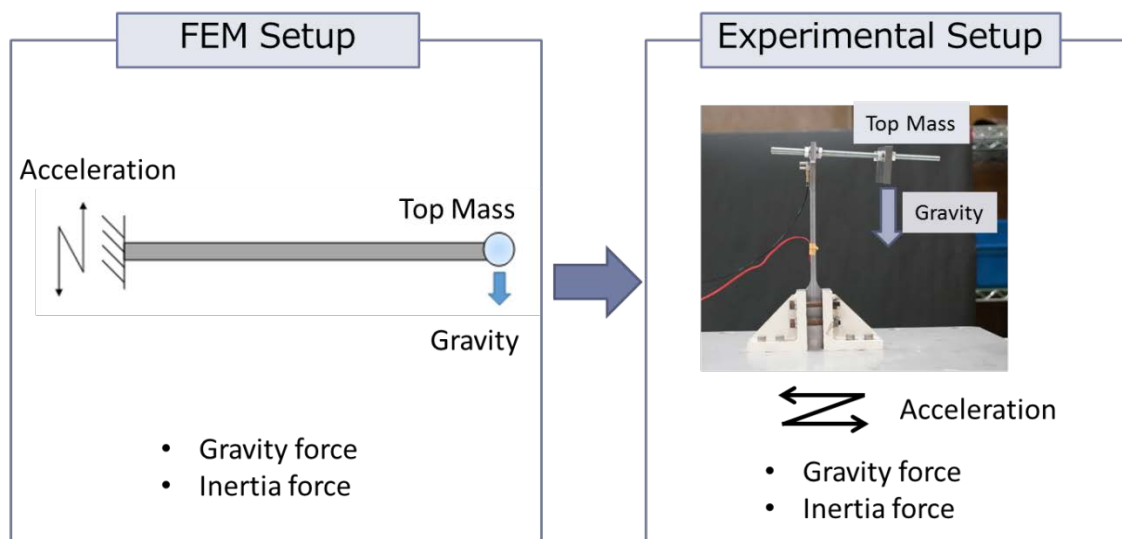


Figure 2-7 Experimental setup followed by FEM setup

2-2-1 Experimental specimen and material

The beam shape specimen has been analyzed in experimental analyses. The geometry of the beam specimen is same as FEM model; rectangular beam with a cross-section of 6 X 13 mm was used. The effective length of the beam was 140 mm. An extended part in base was also

provided for holding the specimen into the shaking table and the top of the specimen has extra part to hold the additional mass. The model is shown in Fig. 2-8. The experiments were carried out by a shaking table shown in Fig. 2-9.

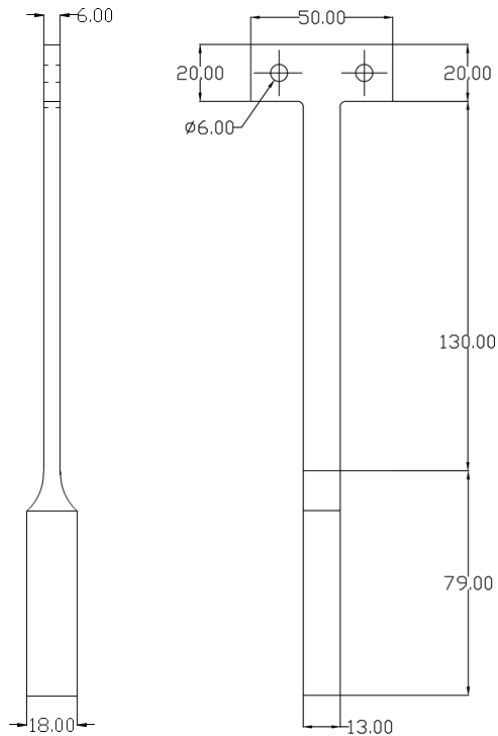


Figure 2-8 Configuration of beam shaped specimen for experiment

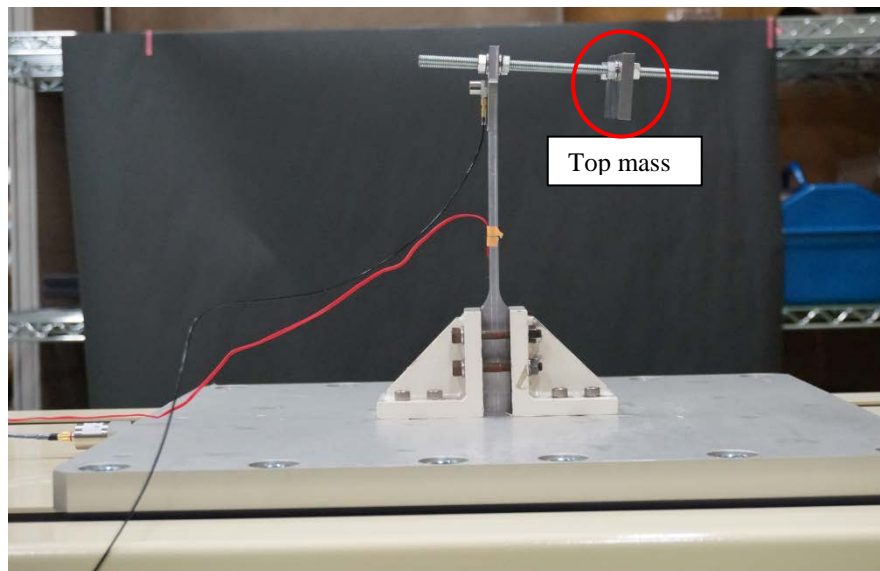
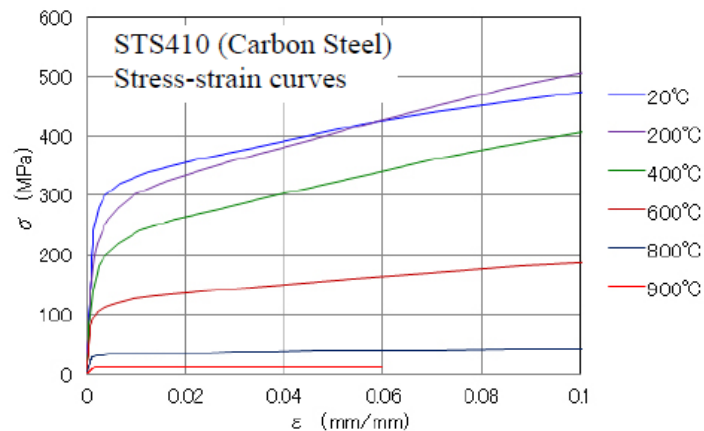


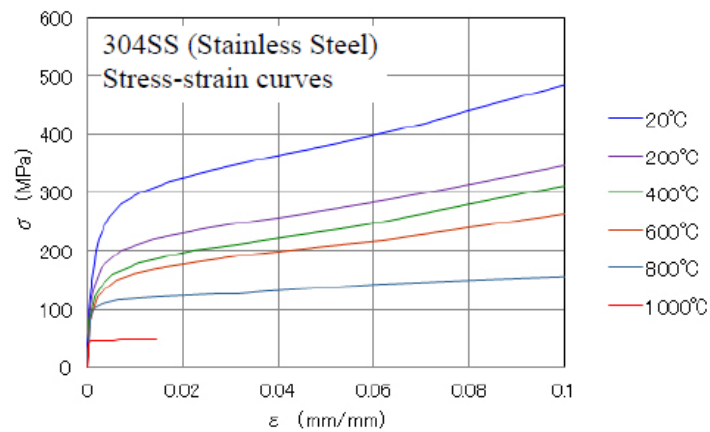
Figure 2-9 Experimental setup

The material of the experimental analysis was same as FEM analysis which was Lead (Pb) or Lead-alloy. In the industrial context the pipes or structure is generally made by steel or iron based metal. But in practice it is difficult to accomplish failure of the structures in laboratory experimental facility with specimens made of steel. This is why, it has been trying to reduce the strength of specimens by using a simulated material to get failure easily. Figure 2-9 shows the stress-strain curves of the steels typically used in nuclear power plants and of simulation materials. It can be seen that in the figure that the stress-strain profile are quite similar, the yield stresses of Pb and Pb-Sb alloys are less than 10% those of steel. It was expected that the mechanical behaviors governed by the stress-strain relationship between actual and simulation materials would be analogous. By using Pb-Sb alloy the external loading needed for failure was reduced so that our laboratory testing facility could use for failure modes evaluation. Finally, the failure mode map has been constructed by using non-dimensional stress parameter which is independent of material

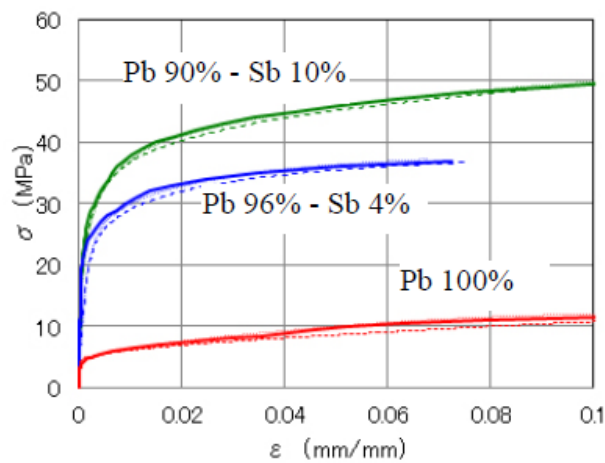


properties.

(a)



(b)



(c)

Figure 2-10 Stress-strain curves of typical structural material (a & b) and simulated materials (Pb-Sb) alloys (c) [58]

Table 2-6 Material properties of Pb (99%) - Sb (1%)

Material	Pb 99% - Sb 1%
Young's Modulus, E	16 GPa
Yield stress, S_y	8.5 MPa

2-2-2 Shaking table and other instruments

The shaking table

The shaking table used mostly in this study is made by SAN-ESU.CO., Ltd, Japan. The model number is SPTD-8KS-85L-5T (shown in Fig 2-11). The maximum acceleration it can generate is about 100 m/s^2 , though it depends on the weight of the specimen. For light specimen it can go up to 100 m/s^2 , whereas for very heavy specimen like 100 kg or more the acceleration decreases to 50 m/s^2 or so on. The shaking table has central processing unit, from where it gets input acceleration. The central processing unit can be seen in Fig 2-12. The upper part of the machine (upper aluminum color part) is moving when there's any input acceleration. An accelerator pickup is attached with moving parts to measure the actual acceleration of base of this machine.



Figure 2-11 Vibration testing machine

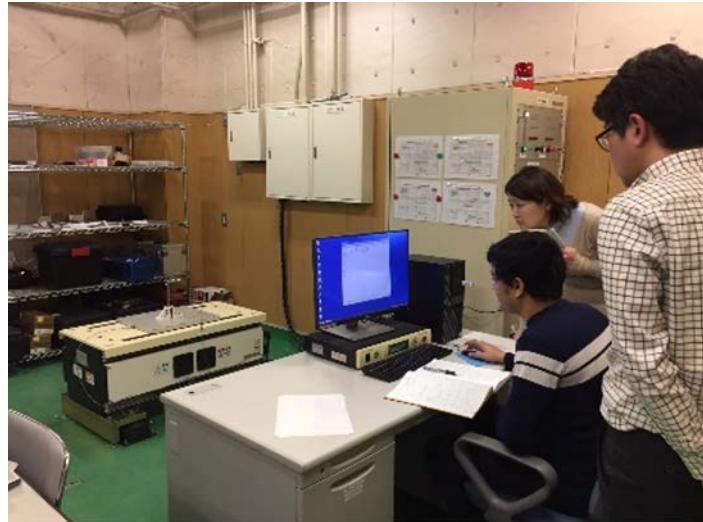


Figure 2-12 Vibration testing machine operation

Data Logger

Data logger is used to collect data of strain during experiment. Keyence data logger was used in this experiment. The Fig 2-13 shows the data logger used in this study.



Figure 2-13 Data logger (Keyence) used in this experiment

Strain gauge

The strain gages used in this experiment are made by KYOWA ELECTRONIC INSTRUMENTS CO., LTD. This is a Japanese company. The model of the strain gage is KFEL-2-120-C1L3M2R. Gage length is 2 mm. Gage is attached with the specimen by appropriate bonding adhesive mentioned in the gage manual.

Acceleration pickup

The acceleration pickup sensors are provided with the shaking table. It is a piezoelectric type accelerometer. Piezoelectric accelerometer employs the piezoelectric effect of certain materials to measure dynamic changes in mechanical variables (e.g., acceleration, vibration, and mechanical shock). Two different accelerometers are used in the experiment. One is fixed with shaking table, this one is pressure type. It is screwed with the base of the shaking table, shown in Fig 2-14. Another accelerometer is attached with the top part of the specimen to measure the response acceleration of the specimen. This one is attached with the specimen by two sided tape.



Figure 2-14 Acceleration pickup (red circle) attached with shaking table

2-2-3 Experimental procedure

To clarify the possible failure modes and to get the occurrence condition of each of the failure modes, the experiments have been carried out. The shaking table experiments also needed to validate the finite element results. The specimen was used mentioned in Section 2-2-1. Additional top mass was placed at the top of the specimen by an offset position to get a desired gravity loading. Figure 2-9 shows the position of additional top mass. The shaking table produced the desired waveforms from the input waveforms. The waveforms used in this study were mainly sinusoidal with varying frequency. The waveforms were tapered at the beginning and end of the steady amplitude. The tapered part is about 10 to 15 % of the total length of waveforms. Generally the number of cycles of each of the waveform was 50, among these 50 cycles 5 to 6 cycles was tapered, it depends on the input frequency and some functions of the software. The waveforms

were generated in the built-in software provided with the shaking table. This was our first attempt to conduct experiment on these failure modes, so the input parameters were changed by trial and error basis. The input parameters were three, the top additional mass, the input acceleration and the frequency of input acceleration. Due to each top mass, the input acceleration was changed to get desired failure. During this time the frequency was unchanged. After that the frequency was changed and repeats the whole procedure. All the experiments were done at room temperature and in our laboratory experimental facility.

Chapter 3 - Ratcheting Failure Mode

3-1 Theory of Ratcheting

Ratcheting is the progressive deformation due to the combined effect of primary and secondary loads [56]. Ratcheting occurs where there is a combination of two different loading, namely- constant primary loading and cyclic secondary loading. If these two loads are high enough, the structure can exhibit an accumulation of plastic strain in each cycle. The ratcheting mechanism of a pressurized cylinder subjected to cyclic thermal stresses was investigated by Miller [57], Bree [56]. The classical case of structural ratcheting diagram is known as Bree diagram. Like other failure modes such as fatigue and creep, ratcheting has also been considered in many design criteria in many structural engineering code, including ASME Code Section III [58], KTA[59], EN13445[60], R5 [61] and RCC-MR [62]. These criteria require the structures to remain below the defined ratcheting boundaries where elastic or plastic shakedown occurs [63]. However, current methods to determine the ratcheting boundaries can be too conservative, or sometimes non-conservative. It is therefore worth to investigate the ratcheting behavior and predict the ratchet boundary with accuracy, which has already been a interest for the researcher for last two decades.

In general, there are three types of modes of ratcheting[64]. First mode (mode I) ratcheting is due to the both membrane primary and secondary stresses without any bending. This type of ratcheting can be modeled by a two-bar structure. The second type (mode II) ratcheting can occur due to the combination of primary membrane stress and secondary bending stress. This type of ratcheting was analyzed by Bree and the proposed diagram is Bree diagram [56]. Finally, mode III ratcheting occurs by the combination of primary and secondary bending loading. The third type of ratcheting is more relevant in the case of seismic loading with gravity load. The third type of

ratcheting is analyzed by Yamashita *et. al.* for bellows. The most simplest ratcheting model are for mode I which has analyzed by two-bar model. The most common and used ratcheting model is the Bree diagram; it is adopted in the ASME Boiler and Pressure Vessel Code. The details of these two models are presented below.

3-1-1 Bree Diagram [56]

Bree analysis is a classical analysis of ratcheting problem. Bree has proposed his diagram in 1967. Currently Bree diagram is extensively used in nuclear pressure vessel industry to delineate the boundaries between various elastoplastic regions. The Bree diagram shows, on a plot of primary stress and secondary stress range, the regions in which ratcheting, shakedown and cyclic plasticity occur. Although derived only for a very simple example problem, the Bree diagram is representative. Bree diagram not only shows the different regions which represent different behavior of stress space, but also it provides expression for ratchet strain and the cyclic plastic strain range. In Bree problem, a thin walled cylinder of an elastic perfectly plastic material is subjected to a fixed internal pressure, P , and a cyclic radial temperature difference ΔT between the inside and outside walls[r]. The resulting Bree diagram is shown in Fig 3-1. The ordinate is the ratio of thermal stress (σ_t) due to temperature difference, ΔT , to the yield stress (σ_y) of the metal and abscissa is membrane stress (σ_p) due to constant internal pressure, P , to the yield stress (σ_y) of the metal. For this configuration, the elastic domain is defined by $\frac{\sigma_p}{\sigma_y} + \frac{\sigma_t}{\sigma_y} = 1$. Except for elastic regime; there are 3 more regions obtained [r].

- (1) **Shakedown regime** localized plastic deformation that occurs in the early stage of cyclic loading gives rise to residual stresses that stabilize the plastic deformation. The consequence is purely elastic behavior during further loading cycles.
- (2) **Alternating plasticity** occurs by loading beyond the shakedown limit. In this regime the plastic strain increment obtained during the first half of each loading cycle is followed by a plastic strain increment of equal magnitude but opposite sign during the second half. No net strain accumulates during each cycle. Alternative plasticity is responsible for low-cycle fatigue.
- (3) **Ratcheting** refers to the condition in which a net increment of plastic strain accumulates during each cycle. The final form of ratcheting is plastic collapse.

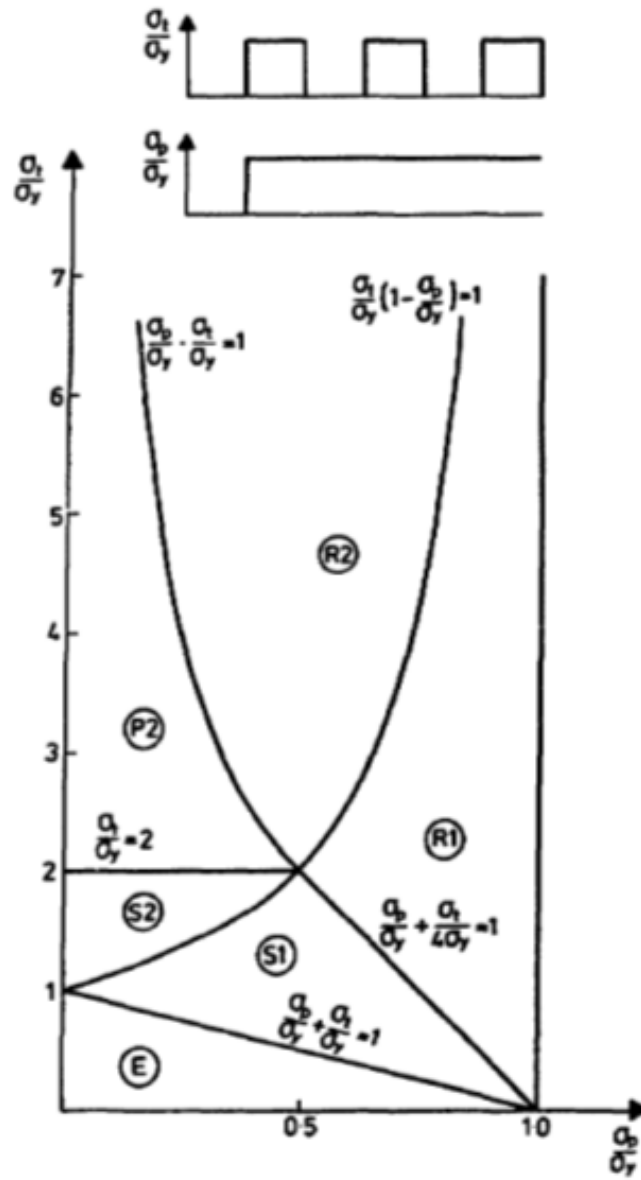


Figure 3-1 Bree diagram for a thin tube [56]

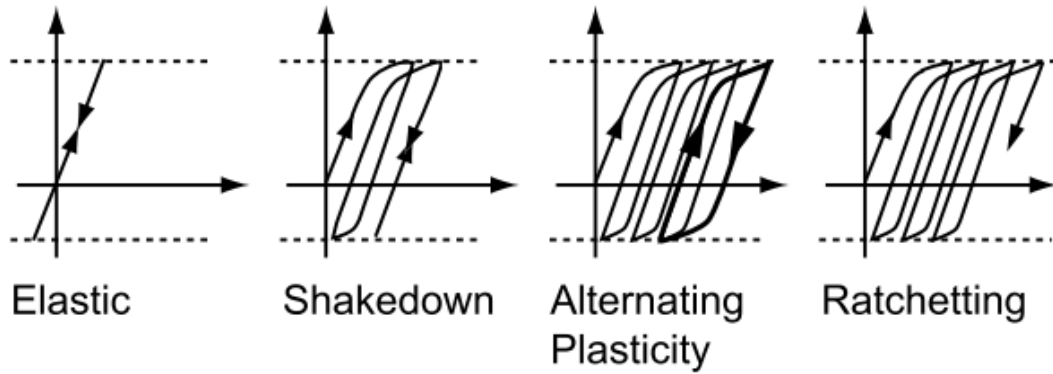


Figure 3-2 Prototypical stress-strain behaviors for an elastic-plastic material in the classic Bree problem [65]

There are total 2 types of ratcheting possible for this loading sequence. In both cases, there is a central core of thickness $2a$ that yields in tension in both halves of each cycle. For R1, a region of thickness $\frac{t}{2} + a$ extending from the outer cooler surface yields in tension while the rest of the thickness remains elastic during one half of the cycle, whereas a region of same thickness extending from the inner surface yields in tension while the rest of the thickness remains elastic during the other half of the cycle. There is no cyclic plastic strain in the tube. The ratcheting strain per cycle for this case is given by

$$\frac{\Delta \epsilon_p}{\Delta N} = \frac{2}{E} [\sigma_t - 2\sqrt{\sigma_y - \sigma_p}] \quad 3.1$$

For region R2, a thin zone at the inner hot surface also yields in comparison during one half of the cycle and a similar zone at the outer surface also yields in compression during the other half of the cycle, so that both surfaces experience cyclic plastic strains. The ratcheting strain per cycle for this case is given by

$$\frac{\Delta \epsilon_p}{\Delta N} = \frac{2\sigma_t}{E} \left[\frac{\sigma_p}{\sigma_y} - \frac{\sigma_y}{\sigma_t} \right] \quad 3.2$$

The critical condition for ratcheting to occur is the existence of a central core of thickness $2a$ that yields in tension during both halves of the cycle. The boundaries of the ratcheting regime are obtained by setting $a=0$. For alternating plastic cycling (P2) to occur, the mid-surface of the cylinder wall remains elastic, but the elastically computed thermal stress ranges in the two extreme surfaces exceed $2\sigma_y$. The width of the hysteresis loop at a distance x from the mid-surface is given by

$$\Delta\varepsilon_p = \frac{2\sigma_t}{E} [|x| - c] \quad 3.3$$

Where, $c = \frac{2\sigma_y t}{\sigma_t}$ is the distance from the mid-surface to the edge of the reversed plastic zone. The two shakedown zones are characterized by initial yielding in tension (S1) and initial yielding both in tension and compression (S2).

3-1-2 Bending-bending ratchet diagram [64]

Bending-bending ratcheting diagram is proposed by Yamashita *et. al.*[64]. In this analysis the double cantilever beam is subjected to a uniformly distributed constant lateral deflection which is act as primary load and cyclic lateral deflection act as secondary load. The loading and beam model is shown in Fig 3-3.

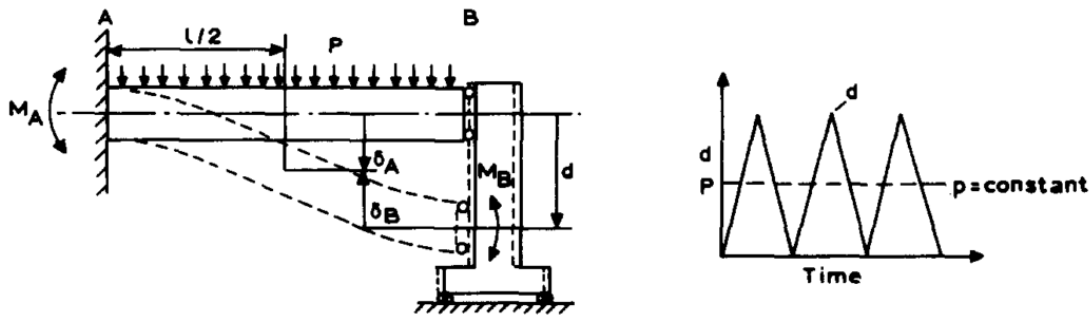


Figure 3-3 Rectangular-beam model for ratcheting [64]

As the primary and secondary loading both are bending, this ratchet diagram is denoted by bending-bending ratchet diagram. The mechanism of ratcheting and other regions of this diagram are expressed by the following moment equations. In these equations the notation P+Q means the application of the primary plus secondary loads and P+Q-Q denotes the subsequent removal of secondary load. Though the analysis is elastic plastic but the basic equations used in this analyses are approximated by elastic analysis. The basic equations are as follows-

$$M_A(P + Q) + M_B(P + Q) = 2M_p \quad 3.4$$

$$M_A(P + Q - Q) + M_B(P + Q - Q) = 2M_p \quad 3.5$$

$$\delta_A(P + Q) - \delta_B(P + Q) = d \quad 3.6$$

$$\delta_A(P + Q - Q) - \delta_B(P + Q - Q) = 0 \quad 3.7$$

Here, M_A and M_B are the elastically calculated bending moment at the two ends and M_p is the end bending moment due to lateral distributed force P. δ_A and δ_B are the end deflection measured at the midspan shown in Fig 3-3.

The mechanism of ratcheting in this case is coming from the bending moment equation of beam. When the bending moment reaches $3/2$ of M_y where M_y is the moment at initial yield. So in this case, when the deflection is sufficiently large, the bending moment at end A reaches the static collapse moment but the bending moment at end B still not reach the collapse moment. This is because the moment at end A is the result of primary plus secondary loading. After the end A reaches the collapse moment, the bending moment at end A and B do not change but the deflection increases until the relative deflection satisfy the equation 3.6. At this time the plastic hinge is created at end A. So the equation becomes-

$$M_A(P + Q) = \frac{3}{2}M_y \quad 3.8$$

$$M_B(P + Q) = 2M_p - \frac{3}{2}M_y \quad 3.9$$

The next step is unloading of load Q. During this time the moment at end A decreases and moment at end B increases. The following three situations can occur in this time-

$$M_B(P + Q - Q) < M_y \quad 3.10$$

$$M_y \leq M_B(P + Q - Q) < \frac{3}{2}M_y \quad 3.11$$

$$M_B(P + Q - Q) = \frac{3}{2}M_y \quad 3.12$$

When the situation satisfies the equation 3.10 and 3.11, shakedown will occur, as the ratcheting can only occur when the moment of end B reaches the collapse moment. Ratcheting will occur when the equation 3.12 satisfies. So the plastic hinge is created at the both ends and plastic bending strains increases at ends A and B alternately in every half cycle. Yamashita *et. al.* describe the ratcheting mechanism of this type of ratcheting is

(1) plastic strains increase at end A and end B alternately in every half- cycle of cyclic deflections;

(2) accumulated strains are bending.

These features correspond completely to those of bellows as the target of this ratcheting analysis is to show the ratcheting mechanism of bellow which is different than Bree analysis of thin pipe. The relation between deflection and bending moment is taken linear due to simplicity as shown in Fig 3-4 (dotted line). In this case the following simple equation can be used –

$$M = M_y + \frac{M_y}{2(K-1)} \left[\frac{\delta}{\delta_y} - 1 \right] \quad \text{for } \delta_y \leq \delta < K\delta_y \quad 3.13$$

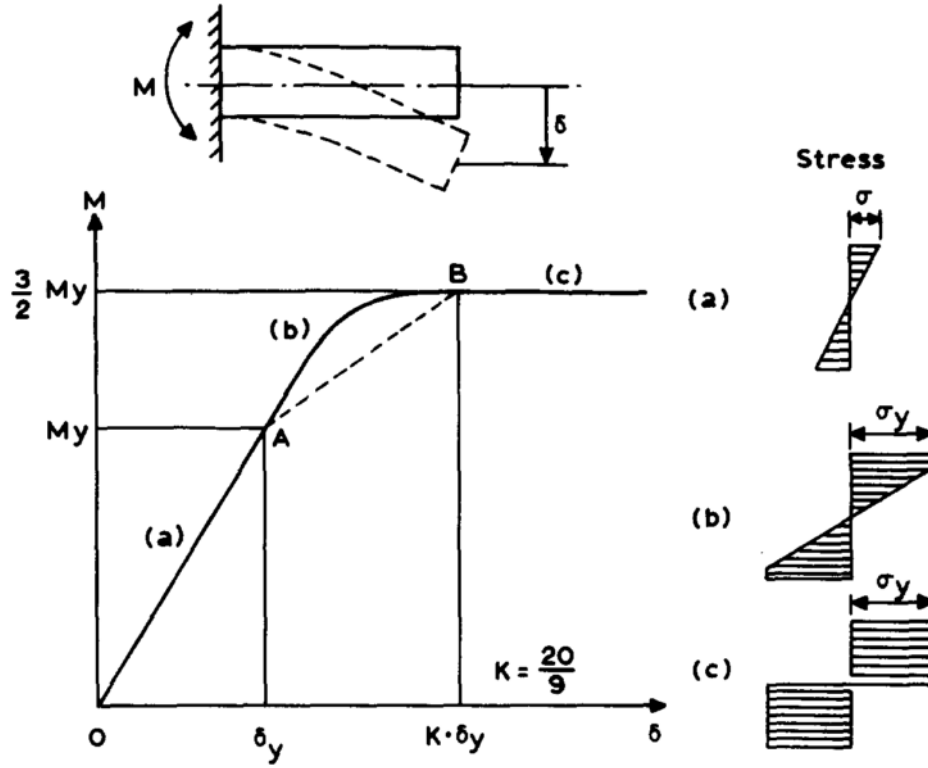


Figure 3-4 Relationship between deflection and bending moment [64]

By using this equation and equation 3.4 to 3.7 along with the primary and secondary load that satisfy the equation 3.10 to 3.12 the following ratchet diagram was constructed -

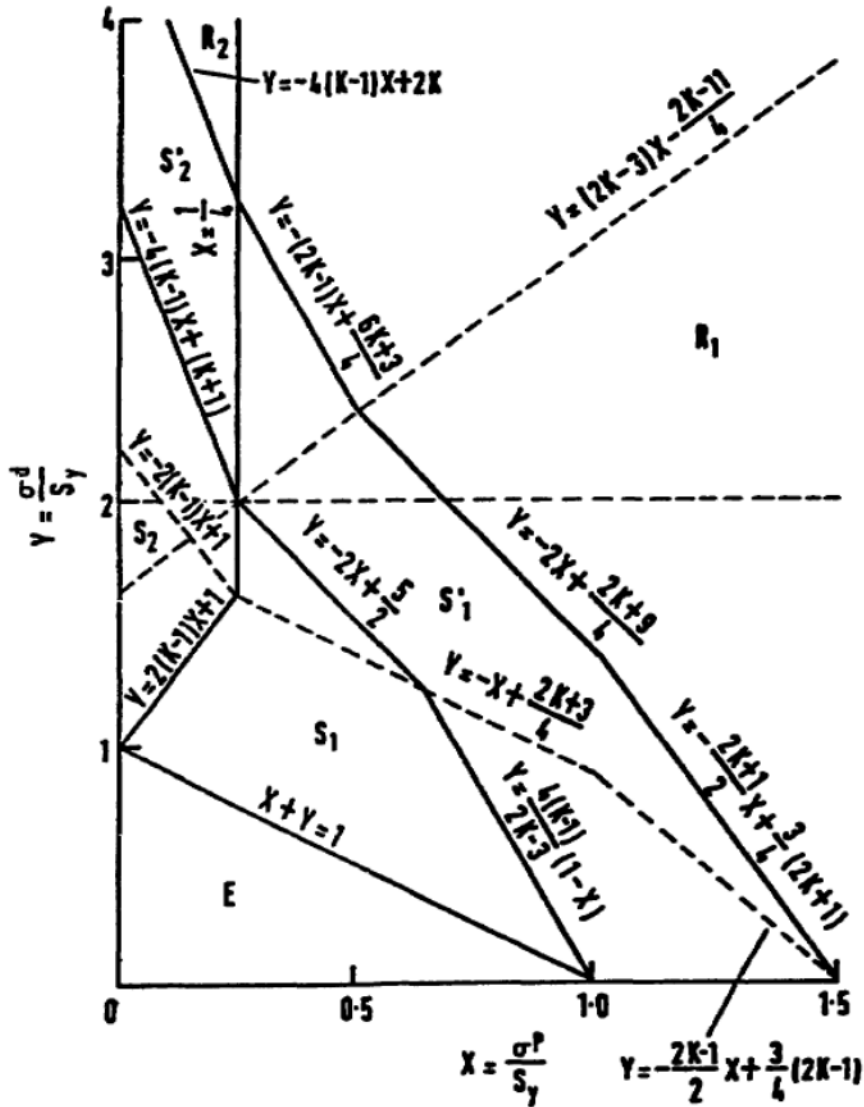


Figure 3-5 Ratchet diagram for rectangular beam [64]

The elastic region, shakedown 1 (S1) and shakedown 2 (S2) regions satisfy the equation 3.10, the regions quick shakedown 1 (S'_1) and quick shakedown 2 (S'_2) satisfy the equation 3.11 and the ratcheting is regions (R1 and R2) satisfy the equation 3.12.

3-1-3 Treatment of seismic loading

In this study, the acceleration was put at the base of the specimen or model. But there was a question, wheatear this acceleration represent the ground acceleration due to earthquake or it was floor response acceleration. To understand the phenomena of earthquake attack to the components the following figure might be helpful.

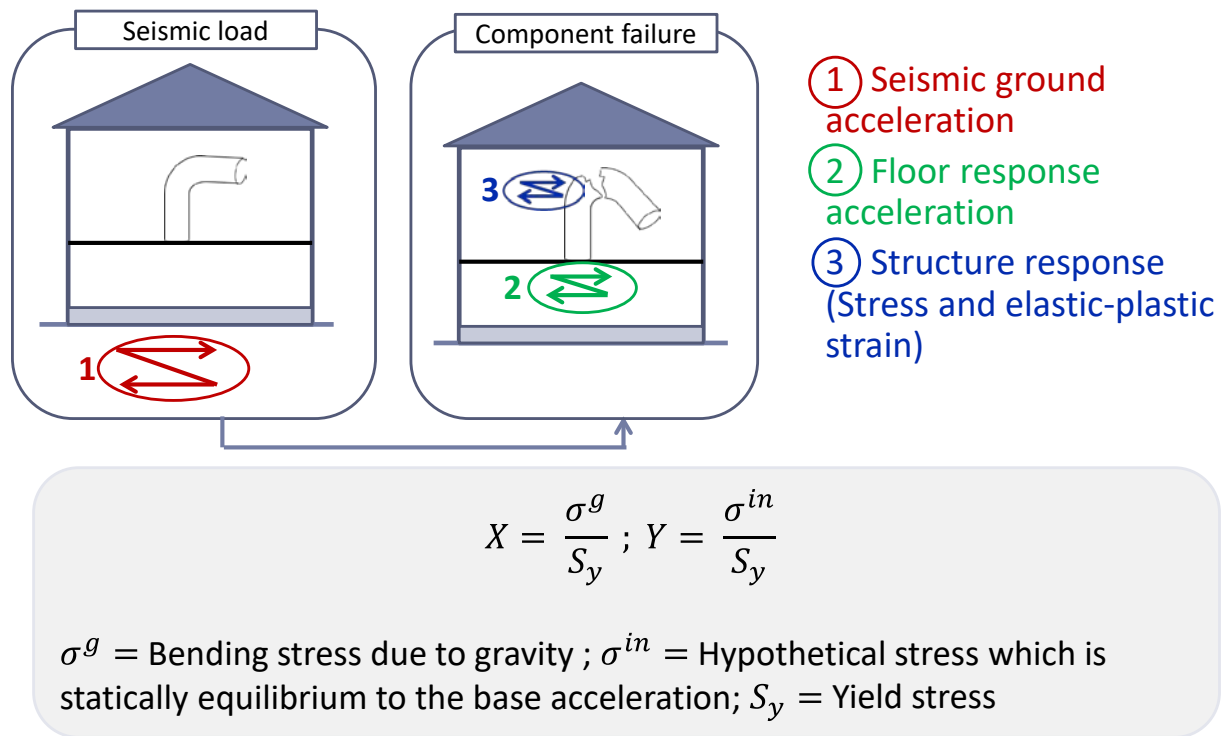


Figure 3-6 Ground acceleration and floor response acceleration

From the figure, it can be seen that the ground acceleration hit the building where the component was installed. The number one acceleration in this case is the ground acceleration. After that, this ground acceleration transferred to the various floor of the building, by a modified acceleration due to the building's own response. This number two acceleration is known as floor response. Finally, due to the floor response, the target components vibrate in another response acceleration which is known as structural response. In this study, the input acceleration is the

number two acceleration or floor response acceleration. One of the objectives of this study is to clarify the different failure modes by putting the occurrence conditions of various failure modes to a non-dimensional stress parameter plot (X,Y plot) similar to Bree diagram. In this case, acceleration is needed to the non-dimensional secondary stress parameter Y. To calculate Y, this research decided to use the floor response acceleration, in other word the input acceleration. There are several reasons to do that. First of all, due to the floor response there will be a structural response on the component. This structural response is a result of the elastic-plastic strain and deformation of the structure, this structural response is caused by the input floor response. As out target is to measure the elastic-plastic deformation (ratcheting, collapse), so it is rational to use the input acceleration rather than structural response acceleration calculated by elastic dynamic response. Secondly, engineering analysis is mainly elastic. Bree diagram consider elastic approximation to calculate Y. By considering floor response acceleration, this calculation also uses statically equilibrium stress to the maximum floor response acceleration. This is the same way as the seismic static force. Another reason is the easiness, if it uses the structural response acceleration, it would be difficult for the engineers or designer to get the structural response acceleration. Because of all these reasons, the calculation of Y value takes statically equilibrium stress to the maximum floor response acceleration rather than structural response acceleration.

3-2 Finite element analyses of beam models

Dynamic elastic-plastic FE analyses were performed using the FINAS/STAR finite element code [52]. FEMAP[51] was used for modelling. The beam model was shown in Fig 2-1 and 2-3 and the details of the model are explained in Section 2-1-1. The target of the beam model analysis is to make a ratchet boundary similar to Bree ratchet diagram. The difference from Bree

diagram to the present study is that, Bree consider membrane load as primary load and thermal bending load as secondary load whereas, in this analysis the primary and secondary both loadings are bending. The loading condition of this analysis is more close to ‘bending-bending’ ratchet diagram by Yamashita et.al., but it also differs from Yamashita’s model by two reasons. One is the secondary load, in the case of Yamashita’s model, the secondary load is cyclic lateral deflection which is a pure displacement-controlled load but in the present model the secondary load is coming from base acceleration due to earthquake. And the seismic load can be act as both load-controlled or displacement controlled loading. Secondly, cyclic lateral deflection doesn’t have any frequency effect but for seismic load is strongly dependent on frequency.

Occurrence condition of ratcheting was evaluated and plotted in a non-dimensional stress parameter X, Y diagram similar to Bree diagram. Where, X is the non-dimensional primary stress parameter, which can be written as

$$X = \frac{\sigma_g}{\sigma_y} \quad 3.14$$

$$Y = \frac{\sigma_i}{\sigma_y} \quad 3.15$$

Here,

σ_g = bending stress due to gravity calculated elastically

σ_i = bending stress due to maximum acceleration calculated elastically

σ_y = yield stress of the material

Bending stresses are calculated by the following equations,

$$\sigma_1 = \frac{M_g}{Z} \quad 3.16$$

$$\sigma_2 = \frac{M_{in}}{Z} \quad 3.17$$

Whereas, M_g and M_{in} are the moments due to gravity and inertia force and Z is the section modulus. The moment due to gravity is calculated by considering the weight of top additional mass and the self-weight of the beam. And the moment due to inertia is calculated by considering the maximum input acceleration.

In these analyses three parameters were taken into consideration. These are-

- ① Steady bending stress by changing the top additional mass to get various X value
- ② Dynamic bending stress by changing the input acceleration to get sufficient Y value for occurrence of ratcheting at each X value
- ③ Frequency of acceleration to investigate the influence of frequency on occurrence of ratcheting. The conditions of ratcheting were examined by changing the acceleration for each of the five kinds of frequencies with eight kinds of top additional weights. The frequencies were the function of natural frequency of each of the model.

The analysis conditions are summarized in Table 3-1

Table 3-1 Analyses conditions of ratcheting of beam model

Case No.	Steady bending stress		Natural Frequency [Hz]	Input frequency [Hz]	
	Top additional mass [kg]	X			
1	0.00	0.22	59.60	0.5fn	29.80
2				1.0fn	59.60
3				1.5fn	89.40
4				1.75fn	104.30
5				2.0fn	119.20
6	0.05	0.40	36.18	0.5fn	18.09
7				1.0fn	36.18
8				1.5fn	54.27
9				1.75fn	63.32
10				2.0fn	72.36
11	0.080	0.50	30.82	0.5fn	15.41
12				1.0fn	30.82
13				1.5fn	46.23
14				1.75fn	53.94
15				2.0fn	61.64
16	0.1	0.57	28.33	0.5fn	14.17
17				1.0fn	28.33
18				1.5fn	42.50
19				1.75fn	49.58
20				2.0fn	56.67

Table 3-1 Analyses conditions of ratcheting of beam model
(continued)

Case No.	Steady bending stress		Natural Frequency [Hz]	Input frequency [Hz]	
	Top additional mass [kg]	X			
21	0.165	0.80	23.10	0.5fn	11.55
22				1.0fn	23.10
23				1.5fn	34.65
24				1.75fn	40.43
25				2.0fn	46.20
26	0.223	1.00	20.28	0.5fn	10.14
27				1.0fn	20.28
28				1.5fn	30.42
29				1.75fn	35.50
30				2.0fn	40.56
31	0.279	1.20	18.34	0.5fn	09.17
32				1.0fn	18.34
33				1.5fn	27.50
34				1.75fn	32.10
35				2.0fn	36.68
36	0.336	1.40	16.85	0.5fn	08.43
37				1.0fn	16.85
38				1.5fn	25.28
39				1.75fn	29.49
40				2.0fn	33.70

Under these conditions, the input wave was a sinusoidal wave of 100 cycles, and it was input as a base excitation at the fixed end of the beam. Figure 3-1 shows an input wave of 100 gal ($= 1 \text{ m/s}^2$) at a natural frequency (23.10Hz) of 0.165 kg as an example, in this figure only 23 cycles were shown to have a clear view of the wave, but in analyses total 100 cycles of input was used.

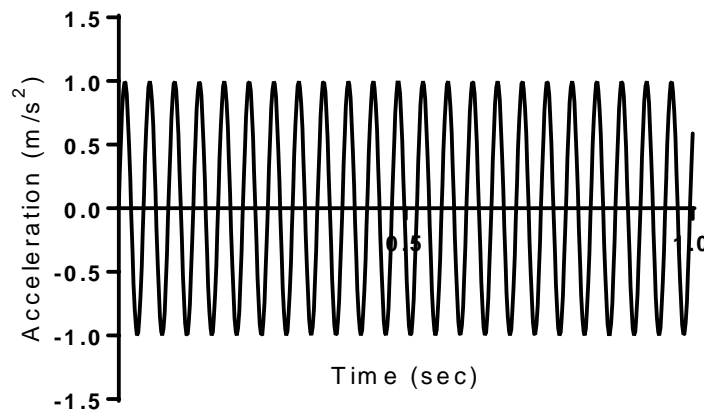


Figure 3-7 Typical input acceleration for ratcheting analyses

3-3 Dynamic experiments of beam models

3-3-1 Experimental conditions of beam models

In order to clarify the ratcheting occurrence conditions by experiment, similar beam shaped model to analysis model of Fig 2-8, has been tested. The beam material was used made of lead alloy (Pb 99%-Sb1%). Due to the limitation of laboratory facilities, it was difficult to accomplish failure with specimen made of steel which is used in actual plant. It is because a large external force is needed for steel to fail which is unable to provide by experimental facility in our laboratory. Excitation tests were conducted to obtain occurrence condition of ratcheting. The test setup is shown in Fig 2-9. The ratcheting occurrence conditions were recorded for mainly four different

frequencies (0.5, 1.0, 1.5 and 2.0 times of natural frequency) at four different gravity loading conditions. The acceleration was adjusted to obtain ratcheting at different conditions as mentioned above.

To get the occurrence condition of ratcheting, similar procedure was taken for experiment as like finite element analyses. The three parameters namely, the steady bending stress, the cyclic dynamic bending stress and the frequency of input acceleration were taken into account for experimental analyses too. As this was the first attempt to conduct experiments, a trial and error methodology was chosen to get the occurrence condition of ratcheting. Since the gravitational force applied to the weight is a static load, the steady bending stress σ_g generated can be calculated by the following beam bending theory.

$$\sigma_g = \frac{M_1}{Z} \quad 3.18$$

M_1 is the bending moment by the weight, and Z is the section modulus. In the shape of the test piece used in this test, Z was measured using width b and height h ,

$$Z = \frac{bh^2}{6} \quad 3.19$$

Since the test pieces used in this test are all similar in shape, the width b is 13 mm and the height h is 6 mm. The bending moment M_1 by the weight is calculated by using the additional mass m_{mass} , the rigid rod mass m_{lod} , the length of the link l_{mass} up to the weight and the length l_{lod} to the center of gravity of the rigid rod and the gravitational acceleration g ,

$$M_1 = m_{mass} * g * l_{mass} + m_{lod} * g * l_{lod} \quad 3.20$$

The detail of the shape is as shown in Fig 3-12. Substituting values into Equation 3.20 for each condition of the specimen and substituting the substituted Equation 3.20 and Equation 3.19 into Equation 3.18, the steady bending stress σ_g due to the mass can be obtained.

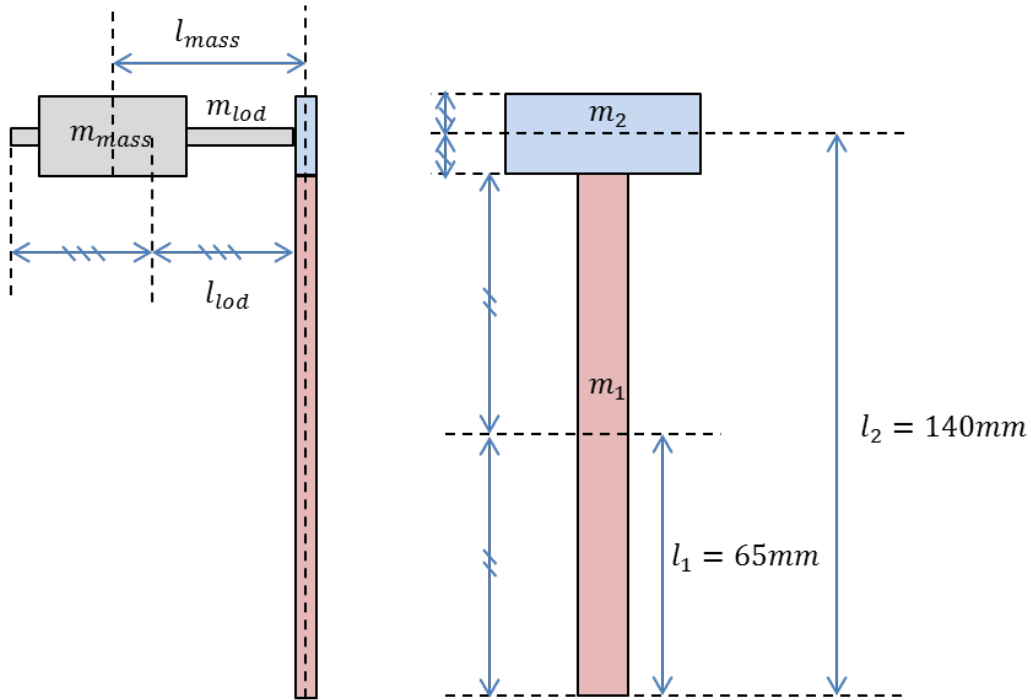


Figure 3-8 Detailed dimension of experimental setup

The input acceleration amplitude of the second parameter will be described. In this case, in order to treat it as equivalent to the first parameter steady bending stress, the input acceleration amplitude is converted into stress. Inertial force acts on the specimen due to the exciting acceleration, which generates bending stress. However, due to the influence of the response characteristic of the structure to the vibrating load, it does not always respond to its inertial force by 1 time. In the test, it is impossible to actually calculate the stress occurring in the test piece due to the vibration load, so here we deal with the magnitude of the inertial force given by the maximum acceleration of the vibration load statically, and the repeated bending stress σ_i is calculated as an apparent stress which is statically balanced with the input acceleration, thereby converting it into the magnitude of the vibration load. First, the bending moment M_2 generated by

the inertial force due to the vibration load is calculated from the input acceleration amplitude a , the additional mass m_{mass} , the test piece mass m_1 and m_2 , shown in Fig 3-12 and the distance of the center of gravity from the base of these test piece masses l_1 and l_2 .

$$M_2 = m_1 a l_1 + (m_{mass} + m_2) a l_2 \quad 3.21$$

The input acceleration amplitude a is the acceleration obtained from the accelerometer installed in the shaking table. Using Equation 3.21, as in Equation 3.18, the repeated bending stress σ_i when converting the vibration load into the bending stress,

$$\sigma_i = \frac{M_2}{Z} \quad 3.22$$

From the above calculation, the steady bending stress due to gravity, σ_g by the first parameter and the second parameter, the input acceleration amplitude was treated as the static inertia force as the magnitude of the inertial force given by the seismic load which is converted to repeated bending stress σ_g . Finally, the plot of experimental results was same as finite element results, a non-dimensional stress plot X, Y. The X and Y can be calculates by using the Equation 3.14 and 3.15.

The following test conditions (Table 3-2) were evaluated for experimental analyses.

Table 3-2 Experimental analyses conditions for ratcheting for beam model

Case No.	Steady bending stress		Natural Frequency [Hz]	Input frequency [Hz]	
	Top additional mass [kg]	X			
1	0.245	0.3272	15.625	0.5fn	7.81

2				1.0fn	15.63
3				1.5fn	23.43
4				2.0fn	31.25
5	0.340	0.5123	11.718	0.5fn	5.85
6				1.0fn	11.72
7				1.5fn	17.58
8				2.0fn	23.44
11	0.530	0.7371	9.375	0.5fn	4.69
12				1.0fn	9.38
13				1.5fn	14.06
14				1.75fn	18.75
16	0.805	1.0626	8.79	0.5fn	4.39
17				1.0fn	8.79
18				1.5fn	13.16
20				2.0fn	17.58

3-4 FE analyses of elbow pipe models

Since the occurrence of ratcheting of beam model was confirmed by the experiment and validation of finite element method was also done. The similar finite element method was extended to predict the ratcheting behavior of realistic components of nuclear power plant like elbow pipe. The FEM model of the elbow pipe is shown in Fig 2-4, and the details of the model has been discussed in Section 2-1-4 and 2-1-5. The loading condition was similar to the beam model and discussed in Section 2-1-6. The geometry of the model is taken from the experimental model of Nakamura *et. al.* trial model test [44].

Apart from geometry the material modelling was also different of elbow model analyses than beam model. The material model was a linear approximation (bilinear) up to the strain of 5%

in the stress strain diagram of lead shown in Fig 2-5, the work hardening coefficient was set to 50 MPa and kinematic material modelling was used. Elements were analyzed in consideration of shell elements and geometric nonlinearity. Dynamic elastic plastic analyses were carried out on the following analyses conditions.

Table 3-3 Analysis conditions of ratcheting of elbow model

Case No.	Steady bending stress		Natural Frequency [Hz]	Input frequency [Hz]	
	Top additional mass [kg]	X			
1	3.5	1.27	4.05	0.5fn	2.03
2				1.0fn	4.05
3				1.5fn	6.08
4				2.0fn	8.10
5	3.0	1.12	4.30	0.5fn	2.15
6				1.0fn	4.30
7				1.5fn	6.45
8				2.0fn	8.60
9	2.5	0.96	4.62	0.5fn	2.31
10				1.0fn	4.62
11				1.5fn	6.93

12				2.0fn	9.24
13	1.5	0.65	5.53	0.5fn	2.77
14				1.0fn	5.53
15				1.5fn	8.30
16				2.0fn	11.06

Subsequently, ratcheting occurrence conditions are organized by bending stress σ_g due to gravity and bending stress σ_i by inertial force. Stresses were evaluated by the following procedure.

The moments M_1 and M_2 generated in the elbow pipe portion due to gravity and inertia force were obtained by adding together the moments of all the sections of the model like the following-

$$M_1 = \sum m_i \times g \times \Delta x_i \quad 3.23$$

$$M_2 = \sum m_i \times a \times \Delta y_i \quad 3.24$$

Where x is the distance from the center of gravity of the elbow part to the center of gravity of the target member on the axis perpendicular to the direction of gravity, and y is the distance from the center of gravity of the elbow part to the direction of the base excitation. It is the distance from the center of gravity of the elbow on the axis to the center of gravity of the target member position. These were obtained from the figure. Also, g represents gravitational acceleration, a represents input acceleration amplitude, and m represents weight of each member. The bending stress generated by this moment is obtained by the following equation

$$\sigma_g = \frac{M_1}{Z} \quad 3.25$$

$$\sigma_i = \frac{M_2}{Z} \quad 3.26$$

Here, Z is the section modulus, and in the cross-sectional shape of the hollow cylinder, it was given by

$$Z = \frac{\pi}{32} \left(\frac{D_o^4 - D_i^4}{D_o} \right) \quad 3.27$$

The parameters X and Y obtained by the standardized values obtained by dividing σ_g and σ_i obtained by this by the yield stress were obtained.

$$X = \frac{\sigma_g}{\sigma_y} \quad 3.28$$

$$Y = \frac{\sigma_i}{\sigma_y} \quad 3.29$$

Also, the plastic section modulus Z_p at which the entire cross section is in the plastic state is given by the following equation.

$$Z_p = \frac{D_o^3}{6} \left\{ 1 - \left(1 - \frac{z_t}{D_o} \right)^3 \right\} \quad 3.30$$

In the case of the elbow pipe experiment used in this study, it has seen that the plastic collapse occur when the applied moment to the yield moment reaches the value of 1.33 which is, $\frac{M_p}{M_y} = (Y) = 1.33$. This phenomenon also observed in our finite element analyses. The static collapse occurs when the additional mass was increased to 3.8 kg, which is equivalent to 1.33 to 1.37 when calculated using the above equations 3.23 to 3.29. So, it was confirmed that it almost agrees with the theoretical solution. Therefore, 1.33 was used as the theoretical solution of static collapse in this calculation.

Chapter 4 - Other Failure Modes

4-1 Collapse

Collapse is another failure mode which can occur due to excessive seismic loading. Collapse can be defined as the inability of a structural system to sustain gravity loads in the presence of seismic effect which can be characterized by widespread propagation of failure [66]. Collapse refers to the significant plastic deformation occurrence in the structure or a system as a whole (uncontained plastic flow). It occurs when any plastic region in the elbow grown to a sufficient extent such that the surrounding elastic regions no longer prevent the overall plastic deformation from occurring. This is considering a real failure and structure will unable to perform its function. To make collapse failure the structure doesn't need to undergo full collapse rather it makes the structure unable to function properly. The term collapse generally indicates a catastrophic failure, which can be seen in real seismic events like bridge collapse or building collapse. But to get collapse in FEA is not so easy, especially in the form of deformed structure after the analysis. So there are some collapse models which can predict the structure to have sufficient plastic deformation which will make the structure collapse like strain based model. The collapse load can be used as a realistic basis for design. But, at the collapse load, the structure does not necessarily collapse. Therefore, the adjective "collapse" is not appropriate [67] what we mean by the failure mode name collapse. Various research has been conducted on progressive collapse issue for 4 decades, especially for frame structure for building and concrete [68] [69] [70][71][72][73]. Dynamic effect have impact on progressive collapse failure, some researcher put

emphasize on considering inertia effect on the structure[69], whereas some researcher considered dynamic load redistribution has an impact on collapse failure [74][75].

4-2 Fatigue

Fatigue failure is defined as the tendency of a material to fracture by means of progressive brittle cracking under repeated alternating or cyclic stresses. Fatigue is a progressive damage done by initiation and propagation of cracks. Fatigue is also one of the major failure modes due to seismic loading [30][31][32][33][34][35][36][37][38][39]. This study wants to clarify all three failure modes due to seismic loading by putting the occurrence conditions in a non-dimensional stress parameter plot. But alike ratcheting and collapse, fatigue cannot be understood by observing the strain history diagram or defamation. This is why; the plan was to evaluate fatigue by experiment at the beginning. But due to time constraint only preliminary stage of fatigue experiment conducted until now.

Chapter 5 - Conclusions and Future Work

6-1 Conclusions

The one of the aims of this study is to clarify the characteristics of seismic loading with frequency effects on failure modes. And another objective is to make a failure mode map for dominant failure modes due to seismic loading. The following conclusions have been drawn.

6-1-1 Frequency dependent characteristics of seismic loading

In **Chapter 3**, the ratchet diagram was proposed for rectangular beam models. Rectangular beam models were analyzed to understand the basic mechanism of failure modes, especially ratcheting. The proposed diagram which is shown in **Chapter 3** is shown again below, have been validate by the dynamic experiment conducted in our laboratory, which is shown in **Section 3-3**.

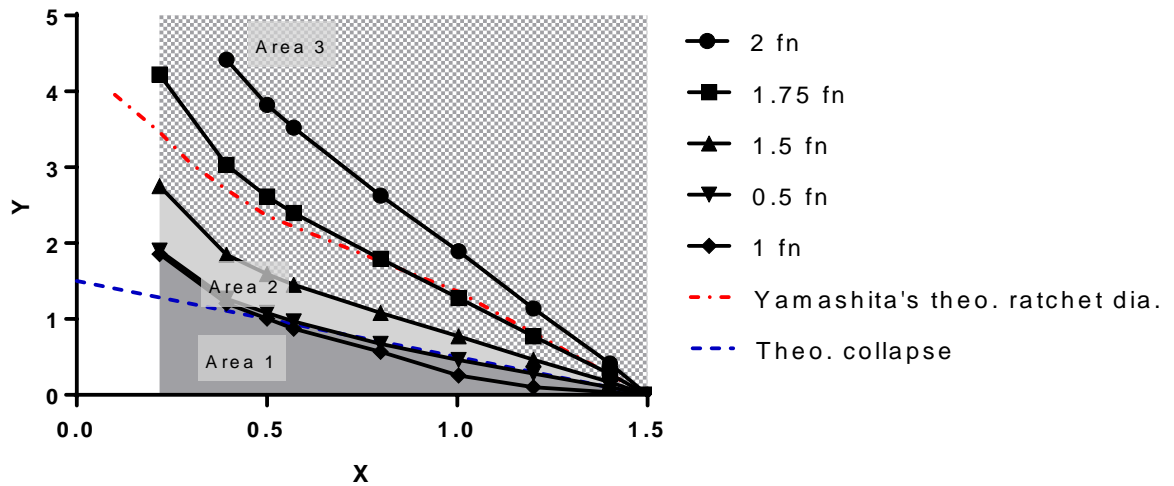


Figure 5-1 Proposed ratchet diagram with theoretical lines

Two distinct characteristics of seismic load have been found. The first one at low frequency, the proposed ratchet boundary follows the theoretical static collapse line. Note that, the theoretical static collapse line is made by pure load-controlled loading. On the other hand, at higher frequency the proposed ratchet boundaries follow the Yamashita's bending-bending ratchet diagram. The secondary load of Yamashita's model is purely displacement-controlled. So, it can be distinguished that at low frequency the seismic load act like load-control loading and at high

frequency the seismic load is more alike of displacement-controlled loading. Further high frequency area has smaller effects on ratcheting than displacement controlled static load.

The reason for this frequency dependent characteristic of seismic loading is also discussed in **Section 3-5**. Two factors have been found to influence the frequency dependency characteristics of dynamic load. The first is the phase difference between the input and the response. When the input frequency is low, the response of the structure follows the input, but as the frequency gets higher, the phase difference gradually approaches the opposite phase, and the transmission of force is delayed and disturbed.

The other factor is energy consumption due to the plasticity cycle, and in the vicinity of the resonance frequency this value becomes very large, the response amplification is lowered and the progressive deformation hardly occurs.

Due to these two effects, failure easily occurs on the low frequency side, but hardly occurs on the high frequency area.

6-1-2 Failure mode map for dominant failure modes

From Section 1-4, it has been seen that ratcheting, collapse and fatigue are the probable failure modes which can occur due to seismic loading. By clarifying the occurrence conditions of these failure modes, the subsequent damage can be stopped in real plants. To realize and understand the effect of various loading on several different failure modes, it is worthwhile to put the occurrence conditions of different failure modes in a same plot which is defined as the failure mode map in this research. The proposed failure mode map which is shown in **Chapter 5** is shown again below.

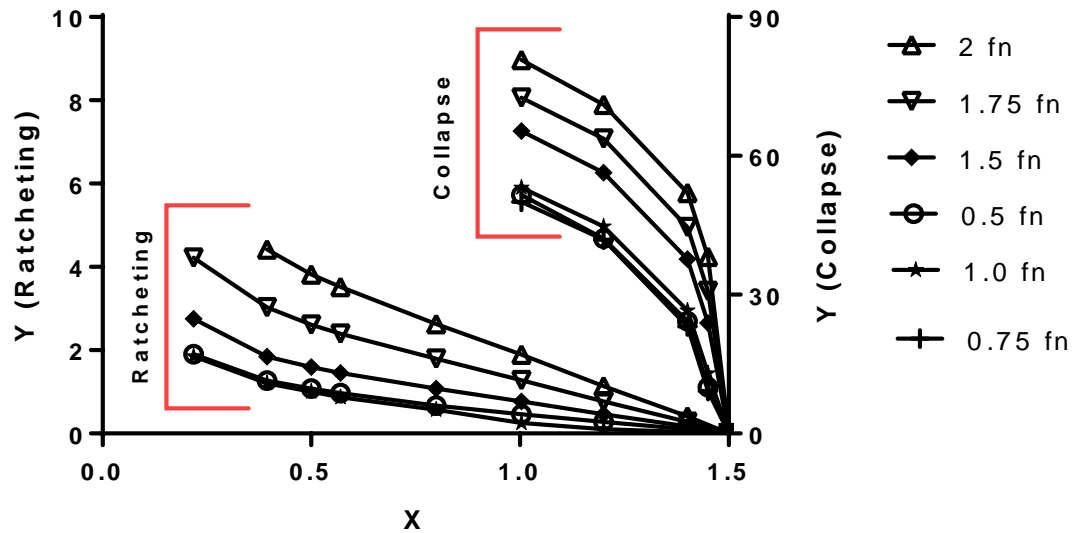


Figure 5-2 Proposed failure mode map

Figure 6-2 is the failure mode map for beam model which includes ratcheting and collapse failure modes. Fatigue will be added in future. Ratcheting and collapse failure modes were analyzed separately and put together here. Failure mode map gives us valuable information regarding which failure modes need to take care when the possible amplitude of seismic loading is known to the designer. The failure modes map can be reshaped if the occurrence conditions of various failure modes changed. The frequency effect can also be visible in failure mode map.

6-1-3 Applicability of simple beam model diagrams to complicated elbow pipe model

The ratchet and collapse diagram for beam model has been evaluated to understand the basic mechanism of these failure modes. As beam model is simple and analytical solutions are available, it is easier to understand the strain and strain evaluation of this structure. This is why; in

this study first the beam model has been analyzed for all the failure modes. The results of beam model are also varied by theoretical results as well as by experimental method. After completing beam analyses, the similar finite element analyses were applied to clarify the occurrence conditions of ratcheting and collapse failure modes. It has been found in Section 3-4 that, the occurrence conditions of ratcheting obtained for beam model is analogous for the ratchet boundaries for elbow pipe model. Similarity has been also found for collapse analyses results as well. In the case of collapse, the occurrence condition of collapse is little different than beam model so the failure diagram also seems little different than beam model, but the trend of the graph is similar in both cases. So, from these analyses, it can be said that the results in the beam model are sufficiently applicable to the elbow piping model.

6-2 Future works

① Investigation of fatigue failure mode

In this study, only preliminary experiments of fatigue failure mode have been done. The fatigue failure mode is one of the major failure modes which can occur due to seismic loading. Due to earlier experimental facility limitations and time constraint, the details fatigue analyses could not be analyzed yet. To complete the failure mode map due to seismic loading, it is necessary to analyze the fatigue failure modes.

② Applicability to realistic seismic load

In this study only the sinusoidal wave is considered even though the realistic seismic wave is random. And finding the effect of frequency was not possible if the input wave was completely random. But the behavior of realistic seismic wave and sinusoidal wave on structure can be different. Therefore, it is necessary to consider the applicability in seismic waves based on the findings by sine wave.

③ More realistic collapse occurrence condition

The collapse occurrence condition used in this study is somewhat unrealistic and it is based on a theoretical model. Practical and more realistic model could make the failure mode map more realistic. The effect of different types of loading on collapse occurrence condition can also be studied in future. Apart from this, the occurrence conditions for ratcheting for elbow pipe model should be optimized. Strain based occurrence criteria can be a solution for all the failure modes. So that the occurrence conditions would be easily understood by all engineers and applicability is easier.

References

- [1] Institute of Nuclear Power Operations, “Special Report on the Nuclear Accident at the Fukushima Daiichi Nuclear Power Station,” 2011.
- [2] International Atomic Energy Agency (IAEA), “Preliminary Lessons Learned from the Fukushima Daiichi Accident for Advanced Nuclear Power Plant Technology Development,” 2013.
- [3] Y. Hatamura, S. Abe, M. Fuchigami, and N. Kasahara, *The 2011 Fukushima Nuclear Power Plant Accident How and Why it Happened*. 2015.
- [4] I. Tokyo Electric Power Company, “Fukushima Nuclear Accident Analysis Report,” 2012.
- [5] M. Ohashi, A. Kasasaki, T. Takeuchi, E. Fujioka, T. Komino, A. Horiuchi, M. Tsukagoshi, and M. Joyce, *10 Lessons from Fukushima - Reducing risks and protecting communities from nuclear disasters*. 2015.
- [6] C. Aa, J. Buongiorno, R. Ballinger, M. Driscoll, B. Forget, C. Forsberg, M. Golay, M. Kazimi, N. Todreas, and J. Yanch, “Technical Lessons Learned from the Fukushima-Daichii Accident and Possible Corrective Actions for the Nuclear Industry: An Initial Evaluation,” 2011.
- [7] Nuclear and Radiation Studies Board, “Lessons Learned from the Fukushima Nuclear Accident for Improving Safety of U.S. Nuclear Plants,” 2014.
- [8] United States Nuclear Regulatory Commission, “NRC: Japan Lessons Learned,” 2016.

- [Online]. Available: <https://www.nrc.gov/reactors/operating/ops-experience/japan-dashboard/priorities.html>. [Accessed: 16-May-2017].
- [9] J. Sugimoto, “Important Severe Accident Research Issues After Accident at Fukushima Daiichi Nuclear Power Station,” in *Volume 6: Beyond Design Basis Events; Student Paper Competition*, 2013, p. V006T15A022.
- [10] United States Nuclear Regulatory Commission, “Recommendations for enhancing reactor safety in the 21th century,” 2011.
- [11] International Atomic Energy Agency, “NS-R-1, Safety of Nuclear Power Plants: Design,” 2000.
- [12] A. Viktorov and C. Harwood, “Design Extension Conditions Concept and its Application to Operating Reactors in Canada,” *Int. Nucl. Saf. J.*, vol. 4, no. 3, pp. 13–23, 2015.
- [13] International Atomic Energy Agency (IAEA), “SSR-2/1 Safety of Nuclear Power Plants: Design,” 2000.
- [14] A. Presidential Task Force on Response to Japan Nuclear Power Plant Events, “Forging a New Nuclear Safety Construct Forging a New Nuclear Safety Construct The ASME Presidential Task Force on Response to Japan Nuclear Power Plant Events,” 2012.
- [15] D. Tecdoc, “Considerations on the Application of the IAEA Safety Requirements for Design of Nuclear Power Plants,” 2014.
- [16] N. Kasahara, I. Nakamura, H. Machida, and H. Nakamura, “PVP2014-28349 RESEARCH

- PLAN ON FAILURE MODES BY EXTREME LOADINGS UNDER DESIGN,” in *Proceedings of the ASME 2014 Pressure Vessels & Piping Conference PVP2014*, 2014, pp. 1–8.
- [17] International Atomic Energy Agency (IAEA), “Safety Reports Series No. 56, Approaches and Tools for Severe Accident Analysis for Nuclear Power Plants,” 2008.
- [18] M. Uesaka, K. Onizawa, N. Kasahara, and K. Suzuki, *Nuclear Structural Engineering*. .
- [19] A. S. of M. E. Committee., ACI-ASME Joint Technical, “Code for Concrete Reactor Vessels and Containments, ASME Boiler and Pressure Vessel Code Section III-Division 2,” 1980.
- [20] C. A. Zalesiak, H. G. Ashar, G. A. Harstead, R. E. Klingner, R. Bandyopadhyay, C. Heinz, D. A. Nuta, R. A. Cook, C. J. Hookham, R. S. Orr, B. Galunic, R. J. Janowiak, B. K. Talukdar, H. L. Graves Iii, J. R. Joshi, D. T. Ward, and A. Y. C. Wong, “Code Requirements for Nuclear Safety Related Concrete Structures (ACI 349-01) ACI 349-01,” 2001.
- [21] and E. of S. S. (AISC) AISC. Specification for the Design, Fabricaiton, “Specification for Structural Steel Buildings,” 2010.
- [22] International Atomic Energy Agency (IAEA), “NS-R-3 Safety Standards Site Evaluation for Nuclear Installations,” 2016.
- [23] H. H. M. Hwang, “Seismic probabilistic risk assessment and seismic margins studies for nuclear power plants,” *Probabilistic Eng. Mech.*, vol. 3, no. 4, pp. 170–178, Dec. 1988.

- [24] M. K. Ravindra, “Seismic probabilistic risk assessment and its impact on margin studies,” *Nucl. Eng. Des.*, vol. 107, no. 1–2, pp. 51–59, Apr. 1988.
- [25] G. E. Cummings and Lawrence Livermore National Laboratory, “Summary report on the Seismic Safety Margins Research Program,” 1985.
- [26] J. B. Savy, “Seismic Hazard Characterization the BNL- H FBR Site (Upton , New York),” 1990.
- [27] J. J. Bommer, K. J. Coppersmith, R. T. Coppersmith, K. L. Hanson, A. Mangongolo, J. Neveling, E. M. Rathje, A. Rodriguez-Marek, F. Scherbaum, R. Shelembe, P. J. Stafford, and F. O. Strasser, “A SSHAC Level 3 Probabilistic Seismic Hazard Analysis for a New-Build Nuclear Site in South Africa,” *Earthq. Spectra*, vol. 31, no. 2, pp. 661–698, 2015.
- [28] D. . Bernreuter, J. B. Savy, and R. W. Mensing, “Seismic hazard characterization of the Eastern United States,” in *Transactions of the 10th international conference on structural mechanics in reactor technology*, 1989.
- [29] R. J. Budnitz, “Current status of methodologies for seismic probabilistic safety analysis,” *Reliab. Eng. Syst. Saf.*, vol. 62, pp. 71–88, 1998.
- [30] K. Fujita, K. Shiraki, K. Kitade, and T. Nakamura, “Vibration Damaged Experiments of Curved Piping for Investigating the Seismic Ultimate Strength,” *JSME*, vol. 44–386, pp. 3437–3445, 1978.
- [31] T. Fujiwaka, R. Endou, S. Furukawa, S. Ono, and K. Oketani, “Study on strength of piping components under elastic-plastic behavior due to seismic loading,” in *ASME PVP*,

- 1999, pp. 19–25.
- [32] S. W. Tagart, Y. K. Tang, D. J. Guzy, and S. Ranganath, “Piping dynamic reliability and code rule change recommendations,” *Nucl. Eng. Des.*, vol. 123, no. 2–3, pp. 373–385, Oct. 1990.
 - [33] F. Touboul, N. Blay, and M. H. Lacire, “Experimental, Analytical, and Regulatory Evaluation of Seismic Behavior of Piping Systems,” *J. Press. Vessel Technol.*, vol. 121, no. 4, p. 388, 1999.
 - [34] G. E. Varelis, S. A. Karamanos, and A. M. Gresnigt, “Pipe Elbows Under Strong Cyclic Loading,” in *Volume 8: Seismic Engineering*, 2012, p. 45.
 - [35] K. Yoshino, T. Sakakida, H. Yokota, and K. Suzuki, “Study on seismic design of nuclear power plant piping in Japan Part 3 ; Component Tests Results,” in *ASME PVP*, 2000, pp. 131–137.
 - [36] K. Takahashi, S. Watanabe, K. Ando, Y. Urabe, A. Hidaka, M. Hisatsune, and K. Miyazaki, “Low cycle fatigue behaviors of elbow pipe with local wall thinning,” *Nucl. Eng. Des.*, vol. 239, no. 12, pp. 2719–2727, 2009.
 - [37] I. Nakamura, A. Otani, and M. Shiratori, “Failure Behavior of Elbows With Local Wall Thinning Under Cyclic Load,” in *Seismic Engineering, Volume 2*, 2004, pp. 173–180.
 - [38] P. K. Singh, V. Bhasin, K. K. Vaze, A. K. Ghosh, H. S. Kushwaha, D. S. R. Murthy, P. Gandhi, and S. Sivaprasad, “Fatigue studies on carbon steel piping materials and components: Indian PHWRs,” *Nucl. Eng. Des.*, vol. 238, no. 4, pp. 801–813, 2008.

- [39] T. J. Katona, “Modelling of Fatigue-Type Seismic Damage for Nuclear Power Plants,” *Open J. Saf. Sci. Technol.*, vol. 2, pp. 41–46, 2012.
- [40] S. W. Tagart, Y. K. Tang, D. J. Guzy, and S. Ranganath, “Piping dynamic reliability and code rule change recommendations,” *Nucl. Eng. Des.*, vol. 123, no. 2–3, pp. 373–385, 1990.
- [41] I. J. Sci and M. Ardabili, “THE RATCHETING RATE OF STAINLESS STEEL PRESSURISED PIPING BRANCH,” *Indian J.Sci.Res.3*, vol. 3, no. 1, pp. 191–199, 2014.
- [42] D. Boussaa, K. D. Van, P. Labbé, and H. T. Tang, “Fatigue-Seismic Ratcheting Interactions in Pressurized Elbows,” *J. Press. Vessel Technol.*, vol. 116, no. 4, p. 396, 1994.
- [43] I. Ichihashi, “SOME COLLAPSE TESTS FOR THE LARGE SCALE MODELS OF THE NUCLEAR REACTOR FACILITIES BY SHAKING TABLE,” *J. Japan Assoc. Earthq. Eng.*, vol. 4, no. 3, 2004.
- [44] I. Nakamura and N. Kasahara, “Trial Model Tests With Simulation Material to Obtain Failure Modes of Pipes Under Excessive Seismic Loads,” in *Volume 8: Seismic Engineering*, 2016, pp. 1–11.
- [45] I. Nakamura, K. Demachi, and N. Kasahara, “AN EXPERIMENTAL INVESTIGATION ON FAILURE MODES OF PIPING COMPONENTS UNDER EXCESSIVE SEISMIC LOAD,” in *SMiRT-23*, 2015, p. 437.
- [46] K. Suzuki, Y. Namita, H. Abe, I. Ichihashi, K. Suzuki, M. Ishiwata, T. Fujiwaka, and K.

- Tai, “Seismic Proving Test of Ultimate Piping Strength: Test Results on Piping Component and Simplified Piping System,” in *Seismic Engineering, Volume 1*, 2002, vol. 2002, pp. 99–106.
- [47] K. Suzuki, Y. Namita, H. Abe, I. Ichihashi, K. Suzuki, T. Sato, and H. Yokota, “Seismic Proving Test of Ultimate Piping Strength (Status of Design Method Confirmation Test),” in *Transactions of the 17th International Conference on Structural Mechanics in Reactor Technology (SMiRT 17)*, 2003.
- [48] K. Suzuki, Y. Namita, H. Abe, I. Ichihashi, K. Suzuki, M. Ishiwata, T. Fujiwaka, and H. Yokota, “SEISMIC PROVING TEST OF ULTIMATE PIPING STRENGTH (CURRENT STATUS OF PRELIMINARY TESTS),” 2004.
- [49] J. P. Bardet and C. Davis, “Engineering observations on ground motion at the Van Norman Complex after the 1994 Northridge earthquake,” *Bull. Seismol. Soc. Am.*, vol. 86, no. 1 SUPPL. B, pp. 333–349, 1996.
- [50] C. Davis and J. P. Bardet, “RESPONSES OF BURIED CORRUGATED METAL PIPES TO EARTHQUAKES,” *J. Geotech. GEOENVIRONMENTAL Eng.*, vol. 126, no. January, pp. 28–39, 2000.
- [51] Structural Dynamics Research Corp., *FEMAP User Guide Version 7.1*. .
- [52] ITOCHU Techno-Solutions Corporation, *FINAS/STAR User Manual*. 2013.
- [53] H. G. Hopkins and A. J. Wang, “LOAD-CARRYING CAPACITIES FOR CIRCULAR PLATES OF PERFECTLY-PLASTIC MATERIAL WITH ARBITRARY YIELD

- CONDITION,” *J. Mech. Phys. Solids*, vol. 8, 1954.
- [54] H. G. Hopkins and W. Prager, “The load carrying capacities of circular plates,” *J. Mech. Phys. Solids*, vol. 2, no. 1, pp. 1–13, Oct. 1953.
- [55] B. S. B. BARKAWI, “FINITE ELEMENT INVESTIGATION OF THE INCREMENTAL DEFORMATION OF COMPONENT,” The University of Nottingham, 1984.
- [56] J. BREE, “Elastic-plastic behaviour of thin tubes subjected to internal pressure and intermittent high-heat fluxes with application to fast-nuclear-reactor fuel elements,” *J. Strain Anal. Eng. Des.*, vol. 2, no. 3, pp. 226–238, Jul. 1967.
- [57] D. R. Miller, “Thermal-stress ratchet mechanism in pressure vessels,” *J. Basic Eng. Trans. ASME*, vol. 81, p. 190–196., 1959.
- [58] American Society of Mechanical Engineers, “Boiler A, Code PV. Section VIII division I, appendix 2,” 2007.
- [59] Teil: Auslegung, Konstruktion und Berchnung, and Regeladerungsentwurf, “Kemteclllischer Allsschu b (KTA). Sicherheitstechnische Regel des KTA,” 1995.
- [60] BS, 2014, ““Unfired Pressure Vessels Part 3: Design,’ (British Standard).,” 2002.
- [61] I. W. Goodall and R. A. Ainsworth, “R5: An Assessment Procedure for the High Temperature Response of Structures,” *IASMiRT*, 1991.
- [62] D. Bonne, O. Gelineau, M. Sperandio, and B. Drubay, “RCC-MR 07 CODE : SPECIFICITIES AND RECENT DEVELOPMENTS,” in *20th International Conference*

- on Structural Mechanics in Reactor Technology (SMiRT 20)*, 2009.
- [63] M. Abdel-Karim, “Shakedown of complex structures according to various hardening rules,” *Int. J. Press. Vessel. Pip.*, vol. 82, no. 6, pp. 427–458, 2005.
 - [64] T. Yamashita, K. Tsukimori, M. N. K. Iwata, and A. Imazu, “A Simplified Method of Evaluating Ratcheting in Bellows and a Test of its Validation,” *Int. J. Pres. Ves. Pip.*, vol. 42, pp. 263–285, 1990.
 - [65] N. Vermaak, L. Valdevit, A. G. Evans, F. W. Zok, and R. M. Mcmeeking, “IMPLICATIONS OF SHAKEDOWN FOR DESIGN OF ACTIVELY COOLED THERMOSTRUCTURAL PANELS,” *J. Mech. Mater. Struct.*, vol. 6, no. 9, pp. 1313–1327, 2011.
 - [66] G. Kaewkulchai and E. B. Williamson, “Beam element formulation and solution procedure for dynamic progressive collapse analysis,” *Comput. Struct.*, vol. 82, no. 7–8, pp. 639–651, 2004.
 - [67] J. T. Boyle, “The design by analysis manual, European Commission, EUR-19030EN,” Brussels, Belgium, 2001.
 - [68] J. Breen, “Research Workshop on Progressive Collapse of Building Structures, Summary report : HUD-PDR-182,” [The Foundation?], [Washington D.C.], 1976.
 - [69] G. Kaewkulchai and E. B. Williamson, “DYNAMIC PROGRESSIVE COLLAPSE OF FRAME STRUCTURES,” in *15th ASCE Engineering Mechanics Conference*, 2002.

- [70] E. Leyendecker and B. Ellingwood, “Design methods for reducing the risk of progressive collapse in buildings,” 1977.
- [71] M. Hakuno, “3D Simulation of Concrete-Frame Collapse due to Dynamic Loading,” in *SMiRT 16*, 2001, p. 1263.
- [72] D. Isobe and Y. Toi, “Analysis of structurally discontinuous reinforced concrete building frames using the ASI technique,” *Comput. Struct.*, vol. 76, pp. 471–481, 2000.
- [73] A. J. Pretlove, M. RAMSDEN, and A. G. ATKINS, “DYNAMIC EFFECTS IN PROGRESSIVE FAILURE OF STRUCTURES,” *Int. J. Impact Eng.*, vol. 11, no. 4, 1991.
- [74] R. B. Malla and B. B. Nalluri, “Dynamic effects of member failure on response of truss-type space structures,” *J. Spacecr. Rockets*, vol. 32, no. 3, pp. 545–551, May 1995.
- [75] R. B. Malla and B. B. Nalluri, “Dynamic nonlinear member failure propagation in truss structures,” *Struct. Eng. Mech.*, vol. 9, no. 2, pp. 111–126, 2000.
- [76] Y. Park and A. H. -S. Ang, “Mechanistic Seismic Damage Model for Reinforced Concrete,” *J. Struct. Eng.*, vol. 111, no. 4, pp. 722–739, Apr. 1985.
- [77] S. Lai, G. T. Will, and S. Otani, “Model for Inelastic Biaxial Bending of Concrete Members,” *J. Struct. Eng.*, vol. 110, no. 11, pp. 2563–2584, Nov. 1984.
- [78] P. S. Rao, B. S. Sarma, N. Lakshmanan, and F. Stangenberg, “DAMAGE MODEL FOR REINFORCED CONCRETE ELEMENTS UNDER CYCLIC LOADING,” *ACI Mater. J.*, vol. 95, no. 6, 1987.

- [79] H. Krawinkler and M. Zohrei, “Cumulative damage in steel structures subjected to earthquake ground motions,” *Comput. Struct.*, vol. 16, no. 1–4, pp. 531–541, Jan. 1983.
- [80] G. Ozcebe and M. Saatcioglu, “Hysteretic Shear Model for Reinforced Concrete Members,” *J. Struct. Eng.*, vol. 115, no. 1, pp. 132–148, Jan. 1989.
- [81] S. K. Kunnath, A. M. Reinhorn, and Y. J. Park, “Analytical Modeling of Inelastic Seismic Response of R/C Structures,” *J. Struct. Eng.*, vol. 116, no. 4, pp. 996–1017, Apr. 1990.
- [82] C. A. Zeris and S. A. Mahin, “Behavior of Reinforced Concrete Structures Subjected to Biaxial Excitation,” *J. Struct. Eng.*, vol. 117, no. 9, pp. 2657–2673, Sep. 1991.
- [83] A. Colombo and P. Negro, “A damage index of generalised applicability,” *Eng. Struct.*, vol. 27, no. 8, pp. 1164–1174, 2005.
- [84] T. C. Triantafillou and L. J. Gibson, “Failure mode maps for foam core sandwich beams,” *Mater. Sci. Eng.*, vol. 95, pp. 37–53, Nov. 1987.
- [85] A. Petras and M. P. F. Sutcliffe, “Failure mode maps for honeycomb sandwich panels,” *Compos. Struct.*, vol. 44, no. 4, pp. 237–252, Apr. 1999.

Acknowledgements

First and foremost, I would like to express my deepest gratitude to my supervisor, Professor **Naoto Kasahara**, Department of Nuclear Engineering and Management, for his magnanimous guidance and valuable counsel in execution and completion of the thesis work, without which it would have been simply impossible to carry out the work. I sincerely appreciate for his excellent guidance, caring, patience, and providing me with an excellent atmosphere for doing research.

I would like to thank Associate Professor **Kazuyuki Demachi**, Department of Nuclear Engineering and Management, for his advice and encouragement for this research and my journey to the University of Tokyo.

I would also express my gratitude to Dr. Takuya Sato, Researcher, Kasahara laboratory, Department of Nuclear Engineering and Management, for his valuable guidance and directions in this research. I express my sincere appreciation to former Assistant Professor Byeongnam Jo, Kasahara Laboratory, for his help and guidance in experimental study. Also thanks to Dr. Ritu Bhusal Chhatkuli, Researcher, Kasahara-Demachi laboratory for her valuable advice and help in writing thesis of this research.

Additionally, I would like to thank my committee members Prof. Masakazu Ichimiya, Prof. Tsuyoshi Takada, Prof. Shunichi Suzuki for their interest and insightful comments in my work.

I would also like to convey my thanks our lab secretaries Ms. Ritsuko Mitsubayashi, Ms. Keita Morita for their immense backing and help throughout. My sincere thanks to all the members of vibration group of our laboratory, with whom I had the opportunity to work and collaborate. I would like to thank all the lab members for their help and support.

Acknowledgements

My sincere thanks to all the faculty and staff members of the Department of Nuclear Engineering and Management, the University of Tokyo for their support. It was a real pleasure to work with such lovely people.

I would like to thank the Graduate School of Engineering, the University of Tokyo, for providing me the SEUT fellowship, as a financial support to the successful completion of this research. I would also like to extend the thanks to MEXT for funding and supporting the research program.

At last but not the least, I express my sincere appreciation to my family for their unconditional support, specially my parents for always being there for me.

Finally thanks to all those people who directly or indirectly have contributed to this research.

